Authors' response to the reviews

Once again we would like to thank all of the referees for their comments and suggestions. We have been studying and discussing thoroughly your sharp criticisms and comments which have helped us to identify sections in the manuscript that require supplementing, rewriting or improving. The general referee comments and the evaluation points can be categorised into six major issues. Since these issues are first introduced in the general comments of Referee #1 and then elaborated in one or more of the evaluation points, we suggest to address each issue separately rather than replying to every point. We find that the issues addressed in the general comments and in the evaluation points can be summed up under the following headings together with the changes we have made to the manuscript accordingly:

1. Novelty

One of the major criticisms put forth by the referees was the difficulty of grasping the novelty of our proposed processing method. After all it is not the first time that a seamless DEM across the land-water transition zone has been derived from green LiDAR, and the main processing steps (filtering, water surface detection, refraction…) are unavoidable when processing such datasets. However, we do see our presented work as novel in the ways mentioned below, and we have clarified this in the manuscript:

- We have presented a simple procedure for water surface detection/modelling in the coastal zone using only green LiDAR data. To the authors' knowledge, such processing procedure has not been published before. We have referred to existing published articles that deal with LiDAR data water surface detection/modelling; however, most often NIR LiDAR data are used for the water surface detection, and the few studies dealing with green LiDAR data water surface detection do not go into detail on how to perform the actual modelling of the water surface in a coastal environment.
- The entire method for processing raw green LiDAR data into a DEM has never (to our knowledge) been openly described to such a high level of detail, which makes the processing useful, user friendly, and repeatable. The commercial LiDAR companies have their processing workflows but there is a tendency to keep some steps in their workflows hidden. Therefore we argue that our manuscript in the very detailed description of the workflow provides new knowledge to a broader audience. We have made this clear in the manuscript.
- We have developed a morphological classification based on the processed DEM, thereby adding scientific context to the manuscript (see point 3). We have made our own composition of tools and criteria for the morphological classification, and with this addition we have built a processing procedure that extends all the way from the raw data to classes of morphological features in a coastal environment.

2. Context

A second major issue, addressed by the referees, was the lack of context to the manuscript, and they were absolutely right. Our first submission focused on the technical part of data processing; however, the original project work included also a geomorphological part with a morphometric analysis of the test site. We decided to focus on the technical part in order to provide all details for the community, which is still emerging in the field of airborne green laser scanning and imaging. However, based on the referee comments and suggestions we have decided to include the morphometric analysis in order to demonstrate the application for mapping morphological units in high energy intertidal environments, and specifically in relation to the vast intertidal flats in the Wadden Sea, which are otherwise impossible to map with full coverage in high detail. This addition will further clarify the reason for data collection and processing, which was also an issue addressed by the referees.

3. Morphological quantitative measurements

It was criticized that the originally submitted manuscript was lacking morphological quantitative measurements. We have overcome this issue by adding the morphometric analysis and morphological classification as mentioned in the previous point.

4. Extended discussion

We have consolidated the discussion by relating our developed processing procedure with the state-of-the-art methods of water surface detection and by elaborating more on the scientific implications of our data collection, processing and results. Specifically, we have modified the discussion so it includes:

- A comparison between our water surface detection methods and existing methods.
- The implications of the dead zone.
- The implications of using LiDAR data collected at different days and in different environments for data processing and quality assessment, respectively.
- Our LiDAR data processing method in the context of a morphological classification and the method's transferability to other applications.
- Evaluation and potential of using topobathymetric LiDAR data for mapping morphological features in a highly dynamic tidal environment.

5. More references to relevant literature

The quality and types of references were criticized by the referees in our first submitted manuscript. We have addressed this by including discussion of our method for water surface detection against up to date, peer reviewed published literature on the subject.

6. "Lessons learned"

We addressed this issue in quite few locations in the manuscript when we described the water surface modelling method in detail giving the current achievement and the future work required for enhancing the modelling accuracy via incorporating the wave and slope models in the workflow. We also discussed the choice of thresholds in the morphological classification and showed the importance of choosing the right thresholds for producing the actual morphological features, and concluded that an objective method is required in future work to estimate these thresholds, which renders the method applicable in all environments. We have also demonstrated the ability of green LiDAR to map seamlessly the land-water transition zone with such high accuracy and precision to make it a practical and excellent choice for conducting such work in the coast zone.

We found these six issues to be the major concerns outlined by the referees. The modifications involved in dealing with the issues have required some major amendments, but we are confident that the manuscript has improved.

Thank you for your time reviewing the manuscript and for your suggestions for improving it. We look forward to receive your response to these improvements.

On behalf of all authors,

Faithfully,

Verner B. Ernstsen
Associate Professor
Department of Geosciences and Natural Resource Management
University of Copenhagen, Denmark

Processing and ~~accuracy~~performance of topobathymetric LiDAR data for geomorphometric and morphological classification in ~~land-water transition zones~~a high-energy tidal environment in the coastal zone

M.S. Andersen[1], Á. Gergely[1], Z. Al-Hamdani[2], F. Steinbacher[3], L.R. Larsen[4], V.B. Ernstsen[1]

[1] Department of Geosciences and Natural Resource Management, University of Copenhagen, Denmark

[2] Geological Survey of Denmark and Greenland, Denmark

[3] Airborne Hydro Mapping GmbH, Austria

[4] NIRAS, Denmark

Correspondence to: V. B. Ernstsen (vbe@ign.ku.dk)

Abstract

The transition zone between land and water is difficult to map with conventional geophysical systems due to shallow water depth and often harsh environmental conditions. The emerging technology of airborne topobathymetric Light Detection And Ranging (LiDAR) is capable of providing both topographic and bathymetric elevation information, using only a single green laser, resulting in a seamless coverage of the land-water transition zone. However, there is no ~~standard~~transparent and ~~simple~~reproducible method for processing green topobathymetric LiDAR data into a Digital Elevation Model (DEM). ~~In~~The general processing steps involve data filtering, water surface detection and refraction correction. Specifically, the procedure of water surface detection, solely using green laser LiDAR data, has not previously been described in detail. The aim of this study~~, a~~ was to fill this gap of knowledge by developing a step-by-step procedure for modelling the water surface using the green laser LiDAR data. The detailed description of the processing method ~~is developed for the creation of a~~ augments its reliability, makes it user friendly and repeatable. A DEM ~~based on high resolution~~was obtained from the processed topobathymetric

LiDAR data collected in spring 2014 from the Knudedyb tidal inlet system in the Danish Wadden Sea. The vertical accuracy of the LiDAR data is determined to ±8 cm at a 95% confidence level, and the horizontal accuracy is determined as the mean error to ±10 cm. The LiDAR technique is found capable of detecting features with a size of less than 1 m^2. ~~The created DEM seamlessly covers the land-water transition zone extending down to approximately 3 m water depth which is the maximum penetration depth of the LiDAR system at the given challenging environmental conditions in the Wadden Sea.~~The derived high resolution DEM was applied for detection and classification of geomorphometric and morphological features in the study area. Initially, stage (or elevation in relation to tidal range) was used to divide the area of investigation into the different tidal zones, i.e. subtidal, intertidal and supratidal. Subsequently, a combination of statistical neighbourhood analyses (Bathymetric Positioning Index, moving average and standard deviation) with varying window sizes, combined with the first derivative slope and the area/perimeter-ratio were used to identify and characterise morphometric units. Finally, these morphometric units were classified into six different types of morphological features (i.e. subtidal channel, intertidal flat, intertidal creek, linear bar, swash bar and beach dune). The developed classification method is adapted and applied to a specific case, but it can be transferred to other cases and environments.

1 Introduction

The coastal zone is under pressure from human exploitation in many and various ways. Many large cities are located near the coast, and they grow gradually with the increase in worldwide population and urbanization. Many industrial activities take place in close vicinity to the coast, e.g. fishery, construction, maintenance dredging for safety of navigation, and mining for raw materials. The coastal zone also provides the setting for many recreational and touristic activities, such as sailing, swimming, hiking, diving and surfing. In addition to human exploitation, climate change also poses a future threat with a predicted rising sea level and increasing storm intensity and frequency, expected to cause erosion and flooding in the coastal zone ~~(Mousavi et al., 2011)~~(Mousavi et al., 2011). All these pressures and different interests underpin the societal need for high resolution mapping ~~and~~, monitoring, and sustainably managing of the coastal zone.

~~Traditionally, difficulties of mapping in shallow waters have resulted in an information gap in the~~ The transition ~~zone~~zones between land and water~~, and for that reason there has often~~ have been ~~a demand for~~ difficult or even impossible to map and investigate in high spatial resolution ~~data in the~~

~~shallow water zones (Al-Hamdani et al., 2008). Topobathymetric~~ due to the challenging environmental conditions. The airborne near-infrared (NIR) Light Detection and Ranging (LiDAR) ~~includes~~is a technique often used for measuring high-resolution topography, however, NIR laser is incapable of measuring bathymetry due to the absorption and reflection of the laser light at the water surface. Traditionally, high-resolution bathymetry is measured with a multibeam echosounder (MBES) system mounted on a vessel, but it does not cover the bathymetry in the shallow water due to the vessel draft limitation.

NIR LiDAR and MBES are applied in different environments; however, the data are very similar and the processed high-resolution topography/bathymetry are both often captured in a Digital Elevation Model (DEM). The processed DEM may be applied for various purposes, e.g. for geomorphological mapping. Previous studies classifying morphology in either terrestrial or marine environments have been performed numerous times (Al-Hamdani et al., 2008; Cavalli and Marchi, 2008; Höfle and Rutzinger, 2011; Ismail et al., 2015; Kaskela et al., 2012; Lecours et al., 2016; Sacchetti et al., 2011). These classification studies generally focus on either the marine or the terrestrial environment, and they do not cover the small-scale morphology in the shallow water at the land-water transition zones, due to the challenges of collecting data in these high-energy environments. A new generation of airborne green topobathymetric LiDAR enables high resolution measurements of both topography and shallow bathymetry, and for that reason it is specifically suited to map the land-water transition zone ~~(Guenther, 1985;Jensen, 2009;Pe'eri and Long, 2011)~~(Guenther, 1985; Jensen, 2009; Pe'eri and Long, 2011)~~. The technology~~. The potential of merging morphological classifications of marine and terrestrial environments enables a holistic approach for managing the coastal zone.

Topobathymetric LiDAR is based on continuous measurements of the distance between an airplane and the ground/~~sea bed~~seabed. The distance (or range) is calculated by half the travel time of a laser beam, going from the airplane to the surface of the earth and back to the airplane. The wavelength of the laser beam is in the green spectrum, usually 532 nm, since this wavelength is found to attenuate the least in the water column, resulting in the largest penetration depth of the laser ~~(Jensen, 2009)~~(Jensen, 2009)~~.~~. In literature, topobathymetric LiDAR data is sometimes referred to as either bathymetric LiDAR or Airborne LiDAR bathymetry (ALB). These are just different terms with the same meaning, and in this paper, topobathymetric LiDAR is preferred, since it describes the system's ability to simultaneously measure bathymetry as well as topography.

~~The~~A single laser beam may encounter many targets of varying nature on its way from the airplane and back again, and different processes are influencing the laser beam propagation through air and water. First, the laser beam may be reflected by targets in the air, such as birds or dust particles, and these can show up as LiDAR reflection points in the space between the airplane and the surface. When encountering water, the speed of the laser decreases from 3×10^8 ms^{-1} to e.g. 2.25×10^8 ms^{-1} in 10°C freshwater or e.g. 2.24×10^8 ms^{-1} in 10°C saltwater of 30 PSU ~~(Millard and Seaver, 1990)~~(Millard and Seaver, 1990)~~. Thereby, the total range (R_t) is the mathematical addition of the range in air (R_{air}) and in water (R_{water}) (Mandlburger et al., 2013):.~~

$$R_t = R_{air} + R_{water} = \left(\frac{1}{2} \cdot t_{air} \cdot c_{air}\right) + \left(\frac{1}{2} \cdot t_{water} \cdot c_{water}\right) \quad (1)$$

~~where t_{air}, c_{air}, t_{water}, and c_{water} are laser beam travel time (t) and speed of light (c) in air and water, respectively.~~

The changing speed of the laser beam also affects the direction of the laser beam when penetrating the water surface with an angle different from nadir (Fig. 1) ~~(Guenther, 2007;Jensen, 2009)~~(Guenther, 2007; Jensen, 2009). The laser beam will be refracted according to Snell's Law ~~(Mandlburger et al., 2013)~~(Mandlburger et al., 2013):

$$\frac{\sin\alpha_{air}}{\sin\alpha_{water}} = \frac{c_{air}}{c_{water}} = \frac{n_{water}}{n_{air}} \quad (~~2~~1)$$

where α_{air} is the incidence angle of the laser beam relative to the normal vector of the water surface and α_{water} is the refraction angle in water. n_{water} and n_{air} are the refractive indices of water and air, respectively ~~(Mandlburger et al., 2013)~~(Mandlburger et al., 2013).

The penetration depth in water is limited by the attenuation of the laser beam. Water molecules, suspended sediment and dissolved material all act on the laser beam by absorption and scattering, resulting in substantial reduction in power as the signal propagates into the water ~~(Guenther, 2007;Mandlburger et al., 2013;Steinbacher et al., 2012)~~(Guenther, 2007; Mandlburger et al., 2013; Steinbacher et al., 2012)~~. The laser beam also diverges in the water column, resulting in a wider laser beam footprint, which reduces the resolving capability of small~~. The laser beam also diverges in the water column, resulting in a wider laser beam footprint (Guenther et al., 2000), and this effect reduces the resolving capability of fine-scale morphology the deeper the laser beam penetrates.

The returned signal is represented as a distribution of energy over time, also called the 'full-waveform' ~~(Alexander, 2010;Chauve et al., 2007;Mallet and Bretar, 2009)~~(Alexander, 2010;

Chauve et al., 2007; Mallet and Bretar, 2009). The peaks in the full-waveform are detected as individual targets encountered by the propagating laser beam. If the laser hits two targets with a small vertical difference, such as a water surface and ~~sea bed~~seabed in very shallow water, then the two peaks in the full-waveform may merge together, resulting in the detection of only one target (Fig. 1). This results in a detection minimum of successive returns from a single laser pulse, and the vertical distance within this minimum is referred to as the 'dead zone' ~~(Mandlburger et al., 2011;Nayegandhi et al., 2009)~~(Mandlburger et al., 2011; Nayegandhi et al., 2009). The dead zone is a clear limitation to the LiDAR measurements, which is an important parameter to consider in very shallow water, such as ~~in tidal~~intertidal environments.

The raw LiDAR measurements are spatially visualized as a point cloud, with each point representing an individual target. The point cloud must be piped through a series of steps before it can take shape as a ~~digital elevation model (~~DEM~~). The overall~~ . Most of the processing steps required to process raw topobathymetric LiDAR data to a DEM are ~~known~~similar to the processing steps of topographic LiDAR data (Huising and Gomes Pereira, 1998). However, additional processing steps are required for topobathymetric LiDAR data due to the refraction of the laser beam at the water surface. All submerged LiDAR points have to be corrected for the refraction, but ~~there~~in order to do so, the water depth must be known for each point. This sets a requirement of modelling the water surface before the refraction correction can be performed. The general processing procedure is ~~no~~ well defined; however, there is no standard or universal approach for ~~dealing~~how to deal with ~~the individual steps.~~ these steps. LiDAR companies have their workflows, but the specific steps in their workflow are usually hidden, which make them non-repeatable.

In particular, there is no definitive method for detecting a water surface from ~~the topobathymetric LiDAR data. Careful processing of the LiDAR data is important, in order to obtain the best approximation of the real world in the processed DEM. Finally,~~green topobathymetric LiDAR data. Often the water surface is detected from simultaneous collection of green and NIR LiDAR measurements, where the green laser reflects from the seabed and the NIR laser reflects from the air-water interface, and the NIR laser data are then used to detect and model the water surface (Allouis et al., 2010; Collin et al., 2008; Guenther, 2007; Parker and Sinclair, 2012). The use of NIR LiDAR data for water surface detection has been applied in several studies. For instance, Hofle et al. (2009) proposed a method for mapping water surfaces based on the geometrical and intensity information from NIR LiDAR data. Su and Gibeaut (2009) classified water points from NIR LiDAR based on point density, intensity and altitude. They identified the shoreline based on the

large sudden decrease in NIR LiDAR intensity values when going from land to water. Brzank et al. (2008) used the same three variables (point density, intensity and altitude) in a supervised fuzzy classification to detect the water surface in a section of the Wadden Sea. Another study in the Wadden Sea by Schmidt et al. (2012) used a range of geometric characteristics as well as intensity values to classify water points from NIR LiDAR data.

The capability of NIR LiDAR data for water surface detection is thus well documented. However, deriving all the information (seabed and water surface) from a single green LiDAR dataset would be a more effective solution for water surface detection, with respect to the financial expenses and for the difficulties of storing and handling often very large amounts of data. For this purpose, the Austrian LiDAR company RIEGL have developed a software, *RiHYDRO* (RIEGL, 2015), in which it is ~~essential to determine the accuracy and~~possible to model the water surface in a two-step approach: 1) Classification of water surface points based on areas with two layers (water surface and seabed) and extending the classification to the entire water body, and 2) Generation of a geometric gridded water surface model for each flight swath based on the classified water surface points. However, RiHYDRO is commercial software, and thus the algorithms, which form the basis of the classification and water surface modelling, are not publicly available. Other software packages, such as *HydroFusion* (Optech, 2013) and *LiDAR Survey Studio* (Leica, 2015), also proclaim to have incorporated methods for the entire data processing workflow, but the algorithms in these software packages are also closed and cannot be accessed by users.

Only few research studies have investigated the potential of water surface detection from green LiDAR data. Guenther et al. (2000) even regarded water surface detection from green LiDAR data as unacceptable and they justified it with two fundamental issues: 1) No water surface returns are detected in the dead zone, and 2) Uncertainty of the water surface altitude, because the green water surface returns are actually a mix of returns from the air/water interface and from volume backscatter returns, and they are generally found as a cloud of points below the water surface. Mandlburger et al. (2013) addressed the second issue by comparing the water surface points of NIR and green LiDAR data, and they concluded that it is possible to derive the water surface altitude from the green LiDAR data with sub-decimetre vertical precision ~~of the LiDAR data for assessing the capability of the technique to represent the real world surface.~~relative to a reference water surface derived by the NIR LiDAR data. However, their work addressed only the determination of the water surface altitude, without going into detail on the actual procedure of modelling the water surface. An approach for modelling the water surface from green LiDAR data was presented by

Mandlburger et al. (2015), who did their study in a riverine environment with only few return signals from the water surface. Their method was based on manual estimates of the water level in a series of river cross sections, after which interpolation between the cross sections filled out the gaps with no water surface points to derive a continuous water surface model. The vertical accuracy of the detected water surface was evaluated by statistical comparison against water surface points from a terrestrial laser scanner, resulting in a root mean square error of ±3.3 cm.

~~Develop a processing method~~Published literature that deals with water surface modelling/detection procedure in the coastal zone based solely on green laser Lidar data are very few and the procedure for LiDAR data processing to reach this goal is not clearly explained.

~~The aim of this study is to investigate the potential of topobathymetric LiDAR data to accurately model the real world terrain and surface in land-water transition zones. The aim is achieved by meeting the following objectives:~~

The aim of this study was to investigate the potential of improving the processing procedure of green LiDAR data for generating DEMs in tidal coastal environments characterised by land-water transition zones, and of improving the classification of morphological units in such environments. More specifically, the objectives were:

1. To develop a robust, repeatable and user friendly processing procedure of raw green LiDAR data~~To develop a processing procedure~~ for generating high resolution DEMs~~the generation of a digital elevation model DEM~~ in land-water transition zones.
2. ~~Quantify~~To quantify the accuracy and precision of the green LiDAR data based on object detection.
3. ~~Evaluate the potential of topobathymetric LiDAR to resolve landforms in land-water transition zones.~~
3. To automatically classify morphological units based on morphometric analyses of the generated DEM.

The investigations were based on studies undertaken in a section of the Knudedyb tidal inlet system in the Danish Wadden Sea.

2 Study area

The Knudedyb tidal inlet system is located between the barrier islands of Fanø and Mandø in the Danish Wadden Sea (Fig. 2A). The tidal inlet system is a natural environment without larger influence from human activity. The tides in the area are semi-diurnal, with a mean tidal range of 1.6 m, and the tidal prism is in the order of $175 \cdot 10^6$ m^3 ~~(Pedersen and Bartholdy, 2006)~~(Pedersen and Bartholdy, 2006). The main channel is approximately 1 km wide and with an average water depth of approx. 15 m ~~(Lefebvre et al., 2013)~~(Lefebvre et al., 2013).

~~Three study sites around the tidal inlet system are referred to throughout this work (Fig. 2A-D):~~

~~Study site 1, in which a DEM was generated,~~The study site is an elongated 3.2 km^2 (0.85 × 4 km) section of the Knudedyb tidal inlet system (Fig. 2B). The section is located perpendicular to the main channel and stretches across both topography and bathymetry. The study site extends towards north into an area on Fanø with dispersed cottages (Fig. 2C). The most prominent morphological features within the study site include beach dunes (Fig. 2D), small mounds (Fig. E), swash bars (Fig. 2F-G) and linear bars (Fig. 2H).The quality of the LiDAR data were validated at two sites along Ribe Vesterå River (Fig. 2I-J):

- ~~Study~~Validation site ~~3~~1 is a cement block with a size of 2.50×1.25×0.80 m located on land next to the mouth of Ribe Vesterå River (Fig. ~~2C~~2I). The block was used for assessing the accuracy and precision of the LiDAR data.
- ~~Study~~Validation site ~~3~~2 is a steel frame with a size of 0.92×0.92×0.30 m located in the river with the surface just below the water surface (Fig. ~~2D~~2J). The frame was used for precision assessment.~~Study site 1 extends towards north into an area on Fanø with dispersed cottages (Fig. 2E). The most prominent morphological~~, and for testing the feature detection capability of the LiDAR system. According to the hydrographic survey standards presented by the International Hydrographic Organization (IHO, 2008), cubic features ~~within~~of at least 1 m^2 should be detectable in Special Order areas, which are areas with very shallow water as in the study site ~~include beach dunes (Fig. 2F), small mounts (Fig. G), swash bars (Fig. 2H-I) and linear bars (Fig. 2J).~~.

3 Methods

3.1 Surveys and instruments

LiDAR data and ortophotos were collected by Airborne Hydro Mapping GmbH (AHM) during two surveys on 19 April 2014 and 30 May 2014.

On 19 April 2014, ~~study site 2~~ validation sites 1 and ~~3 was~~2 were covered for accuracy and precision assessment of the LiDAR data by object detection of the block and the frame (for location see Fig. 2). The block was covered by 7 swaths retaining 227 LiDAR points from the block surface. The frame was covered by 4 swaths retaining 46 LiDAR points from the surface of the frame. Ground control points (GCPs) were measured for the four corners of the block with accuracy better than 2 cm using a Trimble R8 RTK GPS. Measurements were repeated three times and averaged to minimize errors caused by measurement uncertainties. GCPs were also collected for the frame; however, during the LiDAR survey the frame experienced an unforeseen intervention by local fishermen using the frame as fishing platform. Therefore, the frame is only used to assess the deviation between the LiDAR points (the precision), and not to assess the deviation between the LiDAR points and GCP's (the accuracy).

On 30 May 2014, the study site ~~1~~ was covered by 11 swaths ~~(Fig. 3),~~ which were used for generating the DEM. Low tide was -1 m DVR90, measured at Grådyb Barre, approx. 20 km NW of the study site.

~~The weather was similar during the two surveys, with sunny conditions, average wind velocities of 7-8 m/s (DMI, 2014a, b) and significant wave heights, measured west of Fanø, of approx. 0.5 m coming from NW (Danish Coastal Authority, 2014). Overall, both days constituted good conditions for topobathymetric LiDAR surveys.~~

The weather conditions were similar during the two surveys, with sunny periods, average wind velocities of 7-8 m/s (DMI, 2014) and approx. 0.5 m wave heights coming from NW, measured west of Fanø (DCA, 2014). The wave heights in the less exposed Knudedyb tidal inlet was observed in the LiDAR data to 0.2-0.3 m. Overall, both days constituted good conditions for topobathymetric LiDAR surveys.

In both surveys, LiDAR data ~~was~~were collected with a RIEGL VQ-820-G topobathymetric airborne laser scanner. The scanner is characterized by emitting green laser pulses with 532 nm wavelength

and 1 ns pulse width. It has a very high laser pulse repetition rate of up to 520,000 Hz ~~and~~, and a beam divergence of 1 mrad creates a narrow laser beam footprint of 40 cm diameter at a flying altitude of 400 m ~~(RIEGL, 2014).~~(RIEGL, 2014), which was the actual flying altitude during the surveys. The high repetition rate and narrow footprint makes it well suited to capture ~~small~~fine-scale landforms ~~(Doneus et al., 2013;Mandlburger et al., 2011;RIEGL, 2014)~~(Doneus et al., 2013; Mandlburger et al., 2011; RIEGL, 2014). An arc shaped scan pattern ~~maintains~~results in a swath width of approx. 400 m (at 400 m flying altitude), while maintaining an almost ~~uniform scan angle of~~ constant 20° (±1~~°), which is influenced by the roll, pitch and yaw of the airplane. This means that the~~°) incidence angle of the laser beam ~~is almost constant at~~ when it penetrates the water surface ~~(Niemeyer and Soergel, 2013)~~(Niemeyer and Soergel, 2013)~~. General specifications of the laser scanner are summarized in Table 1 (RIEGL, 2014;Steinbacher et al., 2012).~~ The typical water depth penetration of the laser scanner is 1 Secchi disc depth.

For each returned signal, the collected LiDAR data contained information of x, y and z, as well as a GPS time stamp and values of the amplitude, reflectance, return number, attribute and laser beam deviation ~~(RIEGL, 2012). Primarily the positions and time stamps of the LiDAR points were used in the data processing. The reflectance, which represents the range-normalized amplitude of the received signal, was used to a lesser extent in the filtering process.~~(RIEGL, 2012).

3.2 ~~From~~Processing raw topobathymetric LiDAR data ~~to~~into a gridded DEM

~~A list of~~The essential processing steps ~~was necessary to produce a DEM from raw~~, which are standard procedure when processing topobathymetric LiDAR data~~.~~, were followed to produce a DEM in the study area. These steps included:

1. Determination of flight trajectory.
2. ~~Integration of sensor data (laser scanner data, motion sensor data, positioning/trajectory data).~~
3. ~~Raw point cloud processing.~~
4. ~~4.~~2. Boresight calibration: Calculating internal scanner calibration.
3. Collecting topobathymetric LiDAR data.
5. ~~5.~~4. Swath alignment based on boresight calibration: The bias between individual swaths was minimized.

~~6.~~5. Filtering: The raw data contained ~~lots of unwanted return signals (~~noise~~)~~ located both above and below ground~~. These points~~, which needed to be filtered from the point cloud.

~~7.~~6. Water surface detection: A water surface had to be established in order to correct for refraction in the following step.

~~8.~~7. Refraction correction: All the points below the water surface were corrected for the refraction of the laser beam.

~~9.~~8. Point cloud to DEM: The points were transformed into a surface ~~which represented~~representing the real world topography and bathymetry.

Step 1 and 2 were performed prior to the LiDAR survey. The different instruments (LiDAR, IMU and GPS) were integrated spatially by measuring their position relative to each other, when mounted on the airplane, and temporally by calibrating their time stamps.

Step 3~~-5 were~~ was the actual LiDAR survey and step 4 was the initial processing ~~steps~~step after the LiDAR survey. ~~A number of reference planes on the ground were measured with RTK GPS, and~~ The bias between the swaths ~~covering these~~ was minimized in the software RiPROCESS (RIEGL LMS) by automatically searching for planes in each swath and then matching the planes ~~were adjusted so that they aligned with the planes. The rest of~~between the swaths~~, which did not cover the reference planes, were aligned with the already adjusted swaths.~~.

Step ~~6-9~~5-8 represents the processing of the point cloud into a DEM. The methods involved in these steps are the main focus in this work and they are described in detail in the following sub-sections. Each swath was pulled individually through the processing workflow to account for the continually changing water level in the study area due to tides.

3.2.1 Filtering

The raw LiDAR data contained ~~a lot of~~ noise ~~points~~ in the air column originating from the laser being scattered by birds, clouds, dust and other particles, and ~~a lot of~~ noise ~~points were~~was also appearing below the ground/~~sea bed~~seabed (Fig. ~~4A~~3A-B). ~~All these~~This noise ~~points~~ had to be filtered before further processing. The filtering process involved both automatic and manual filtering.

1. Automatic filtering

The automatic filtering was carried out in HydroVish (AHM) with the tool *Remove flaw echoes*~~.~~ (Fig. 3C). The filtering tool was controlled by three variable parameters: search radius, distance and

density. The search radius parameter specified the radius of a sphere in which the distance and density filters were utilized. The distance parameter rejected a point, if it was too far from any other point within the sphere. The density parameter specified the lower limit of points within the sphere. The automatic filter iterated through all the points in the point cloud.

In order to identify the best settings of the three parameters, a sensitivity analysis was performed on three data fragments representing different natural environments in the Knudedyb tidal inlet system: a fragment in the flood channel, one on the tidal flat and a fragment with vegetation. The outcome of the filtering was ~~visually evaluated~~compared for different settings to decide the most suitable settings to use for filtering the whole study area. ~~Based on visual inspection of the outcomes, it~~It was ~~impossible~~not possible to reach a specific setting, which would be optimal for all the different environments. Particularly, the deeper bathymetric parts contained more widely dispersed points, which were easily rejected by the filter. The analyses with different settings also showed that two layers of noise ~~points~~ close to the ground, both above and below, were very difficult, if not impossible, to reject with this automatic filtering method. ~~They~~The settings were ~~only rejected if the distance threshold was set very low (0.20–0.25 m) or the density threshold was very large, but~~selected so that ~~would result in~~ a ~~large amount~~minimum of valid points ~~being~~were rejected~~.~~

~~Based on the visual inspection of the filtering sensitivity analysis, the chosen settings for~~ by the automatic ~~filtering~~filter. The settings were: Search radius = 1 m, distance = 0.75 m and density = 4.

2. Manual filtering

The remaining noise ~~points were~~was manually filtered in the software Fledermaus (QPS) ~~based on visual inspection of the point cloud~~ (Fig. ~~4D). The reflectance of the points helped to distinguish between valid and non-valid points.~~3D).

The filtered point cloud (with water points) was used in the following step to detect the water surface. Meanwhile, a copy of the data ~~was~~were undergoing additional manual filtering, removing all the water points (Fig. ~~4E~~3E). After this final filtering step, there were only points representing topography, bathymetry, vegetation and man-made structures left in the dataset.

3.2.2 Water surface detection

The water surface detection was based on determining the water surface ~~*elevation*~~*altitude* and the water surface *extent*. The water surface ~~elevation~~altitude was determined based on the water surface

points and the extent was determined by extrapolating the water surface until it intersected the surface of the topography. Two assumptions about the water surface were made:

1. The water surface was horizontal. This was ~~of course~~ a simplification of the real world. Tidal processes and wind- and wave-setup may cause the water surface to be sloping, and the water is often topped by more or less significant wave action. A linear fit through the water surface LiDAR points along the main channel, showed a changing water level of 0.13 m over a distance of 400 m, corresponding to a 0.325×10^{-3} (0.019 deg.) sloping water surface. A similar fit through the LiDAR points along the flood channel showed a slope of 0.156×10^{-3} (0.009 deg.). The maximum wave heights observed in the main channel were 20-30 cm. Based on the moderate slope of the water surface and relatively low wave height, ~~it was considered acceptable to assume a flat water surface~~the water surface was assumed flat. This assumption is deemed error prone, but at the time of this study, it was currently our best estimate.
2. ~~Study site 1 had~~The study area contained water bodies with two different water levels: One represented the water level in the main channel and the other represented the water level in the flood channel. This was also a simplification, as the tidal flat contained small ~~pools of water~~ponds with potentially different water levels. However, almost all of these ~~pools~~ponds contained no LiDAR points of the water surface, which means that the water depth in the ~~pools~~ponds must have been within the limitation of the dead zone. Therefore, it was impossible to detect individual water surfaces in the ~~pools~~ponds.

A series of processing steps were performed to detect the water surface. The first step was to extract a *shallow surface* and a *deep surface* from the filtered point cloud (with water points) in Fledermaus (Fig. ~~4F~~3F). Both surfaces consisted of 0.5 × 0.5 m cells, and the ~~elevation value in~~altitude of each cell was equal to the highest point within the cell (shallow surface) and the lowest point within the cell (deep surface), respectively. The shallow surface should then display the topography along with the water surface, whereas the deep surface should display the topography and the ~~sea bed~~seabed (as long as the ~~sea bed~~seabed was detected by the laser). It is worth noting, that the extraction of the shallow surface and the deep surface have nothing to do with the final DEM, as they are just intermediate steps performed for the water surface detection.

The following steps were focused on the shallow surface to determine the ~~elevation~~altitude of the water surface (Fig. ~~4G~~3G). First, the shallow surface was down-sampled to a surface with a cell size

of 2 × 2 m, and the new cells were populated with the maximum ~~elevation~~altitude of the input cells. The down-sampling was done for smoothing the water surface, and thereby eliminating most of the outliers. The exact cell size of 2 × 2 m, as well as populating them with the maximum value, was chosen based on the work by ~~Mandlburger et al. (2013).~~Mandlburger et al. (2013). They compared water surface detection capability between green LiDAR data, collected with the same RIEGL-VQ-820-G laser scanner, and ~~near-infrared~~NIR LiDAR data, which was assumed to capture the true water surface. They found that the green LiDAR generally underestimated the water surface level, but that reliable results were achieved by increasing the cell size and only taking the top 95-100% of water points into account. According to their work, it was assumed that placing the water surface on the highest points in 2 m cells provided a good estimate of the true water level. However, based on their results it could be expected that the water surface level in this case would be underestimated in the order of 2-4 cm.

The water covered areas in the main channel and the flood channel were manually extracted from the newly ~~resampled~~down-sampled raster surface. The ~~mean elevation~~average altitude of the cells was calculated individually in each area, and these values constituted the water surface levels in the main channel and in the flood channel, respectively.

Hereafter, the extent of the water surfaces was determined (Fig. ~~4H~~3H). Two horizontal water surfaces ~~was~~were created in the flood channel and the main channel with a cell size of 0.5 × 0.5 m and cell values equal to the determined water surface ~~elevations~~altitudes in each region. The high spatial resolution of 0.5 m cells was chosen to produce a detailed water surface along the edges of the land-water transition. It also made the calculations in the following step straightforward, because the resolution was similar to that of the deep surface. The deep surface cell ~~elevations~~altitudes were subtracted from the water surface ~~elevation~~altitude and all cells with resulting negative values were discarded from the water surface. Thereby, all the water surface cells which were below the deep surface were discarded. All the cells above the deep surface were expected to represent the two water surfaces. Thereby, two water surfaces were created; one in the main channel and one in the flood channel.

3.2.3 Refraction correction

The refraction correction of all the points below the water surfaces was calculated in HydroVish (AHM). The input parameters were the filtered point cloud (without water points), the derived water surfaces and the trajectory data of the airplane. These were all converted to F5 file format to allow

import into HydroVish (AHM). The refraction correction was calculated automatically for each point based on the water depth, the incident angle of the laser beam, and the refracted angle according to Snell's Law (Eq. 1 and Fig. ~~4I~~3I).

3.2.4 Point cloud to DEM

After iterating through the processes of filtering, water surface detection and refraction correction for all the individual swaths, the LiDAR points of all swaths were combined. The transformation from point cloud into a DEM was performed with ArcGIS (ESRI) software. The DEM was created as a raster surface with a cell size of 0.5 × 0.5 m, and each cell was attributed the average ~~elevation of the points within the cell-boundaries. The~~altitude of the points within the cell-boundaries. It was chosen to make the resolution of the DEM lower than the laser beam footprint size (i.e. 40 cm), due to the inaccuracies arising from attributing smaller cells with measured altitude values spanning across a larger area. Furthermore, the 0.5 m cell size was chosen to get as high resolution as possible without making any significant interpolation between the measurements. In this way, each cell represented actually measured ~~elevations~~altitudes instead of interpolated values. However, there were still very few gaps of individual cells with no data in the resulting raster in areas with relatively low point density. Despite of the general intention of avoiding interpolation it was chosen to populate these cells with interpolated values to end up with a full DEM coverage (except for the bathymetric parts beyond the maximum laser penetration depth). The arguments for interpolation were that 1) the interpolated cells were scattered and represented only 1.7 % of all the cells, 2) they were found primarily on the tidal flat where the slope is generally less than 1°, meaning that the ~~elevation~~altitude difference from one cell to a neighbouring cell is usually less than 1 cm, and 3) the general point density in most of the study area was so high that the loss of information by lowering the DEM resolution would represent a larger sacrifice than interpolating a few scattered cells. The interpolation was performed by assigning the average value of all ~~neighboring~~neighbouring cells to the empty cells. The final DEM was thereby fully covering the topography, and the bathymetry was covered down to a depth equal to the maximum laser penetration depth.

3.3 Accuracy and precision of the topobathymetric LiDAR data

The term a*ccuracy* refers to the difference between a point coordinate (in this case a LiDAR point) compared to its "true" coordinate measured with higher accuracy, e.g. by a total station or a differential GPS; while the term *precision* refers to the difference between successive point

coordinates compared to their mean value, i.e. ~~the repeatability of the measurements (Graham, 2012;Jensen, 2009;RIEGL, 2014).~~the repeatability of the measurements (Graham, 2012; Jensen, 2009; RIEGL, 2014).

Two "best-fit planes" based on the LiDAR points on the block and the frame surfaces were established with the *Curve Fitting tool* in MATLAB (MathWorks). ~~These were used to quantify the precision.~~ We propose the use of these two planes to give an indication of the relative precision of the LiDAR measurements.

Another best-fit plane was established based on the block GPS measurements, and this plane was regarded as the "true" block surface for assessment of the accuracy of the LiDAR measurements. The established planes were described by the polynomial equation:

$$z(x, y) = \mathrm{a} + \mathrm{b}x + \mathrm{c}y \quad (3\text{~~2~~}) \tag{3}$$

where x, y and z are coordinates and a, b and c are constants. Inserting x and y coordinates for the LiDAR surface points in Eq. (3) led to a result of the corresponding ~~elevation~~altitude (z) as projected on the fitted plane. The difference between the ~~elevation~~altitude of the LiDAR point and the corresponding ~~elevation~~altitude on the fitted plane was used as a measure of the vertical accuracy (for the GCP fitted plane of the block) and the vertical precision (for the LiDAR point fitted plane of the block and the frame). Statistical measures of the standard deviation (σ), mean absolute error (E_{MA}), and root mean square error (E_{RMS}) were calculated by:

$$\sigma = \sqrt{\frac{\sum(z_{\mathrm{i}} - z_{\mathrm{plane}})^2}{n-1}} \quad (4\text{~~3~~}) \tag{4}$$

$$E_{\mathrm{MA}} = \frac{\sum|z_{\mathrm{i}} - z_{\mathrm{plane}}|}{n} \quad (5\text{~~4~~}) \tag{5}$$

$$E_{\mathrm{RMS}} = \sqrt{\frac{\sum(z_{\mathrm{i}} - z_{\mathrm{plane}})^2}{n}} \quad (6\text{~~5~~}) \tag{6}$$

where z_i is the ~~elevation~~altitude of the measured LiDAR points, z_{plane} is the corresponding ~~elevation~~altitude on the best-fit plane, and n is the number of LiDAR points. The vertical accuracy and precision were determined at a 95% confidence level based on the accuracy standard presented in *Geospatial Position Accuracy Standards Part 3: National Standard for Spatial Data Accuracy* (NSSDA) ~~(FGDC, 1998)~~(FGDC, 1998):

$$CI_{95\%} = E_{\mathrm{RMS}} \cdot 1.96 \quad (7\text{~~6~~}) \tag{7}$$

The horizontal accuracy was determined as the horizontal mean absolute error ($E_{\mathrm{MA,xy}}$) based on the horizontal distances between the block corners, measured with RTK GPS, and the best approximation of the block corners derived from the LiDAR points of the block surface. The minimum distance between a block corner and the perimeter of the LiDAR points was regarded as the best approximation. Hereafter~~,~~ $E_{\mathrm{MA,xy}}$ was calculated as the average of the four corners.

3.4 Geomorphometric and morphological classifications

The processed DEM was applied in two classification analyses; first a *geomorphometric* classification and then a *morphological* classification. Both were based on the DEM and derivatives of the DEM, but they differentiated by the resulting classification classes, which showed 1) Surface geometry and 2) Surface morphology.

Geomorphometric classification analysis

The tool Benthic Terrain Modeler (BTM) (Wright et al., 2005) was used for the geomorphometric classification. The tool is an extension to ArcGIS Spatial Analyst, originally used for analysing MBES data (Diesing et al., 2009; Lundblad et al., 2006; Rinehart et al., 2004). The BTM classification tool uses fine- and broad scale Bathymetric Positioning Indexes (BPIs) (Verfaillie et al., 2007) in a multiple scale terrain analysis to classify fine- and broad scale geometrical features. The BPIs are measures of the altitude of a cell compared to the altitude of the surrounding cells within the determined scale (radius) size. Positive BPI values indicate a higher altitude than the neighbouring cells and negative BPI values indicate a lower altitude than the neighbouring cells. For instance, a BPI value of 100 corresponds to 1 standard deviation and a value of -100 corresponds to -1 standard deviation. BPI values close to zero are derived from flat areas or from constant slopes.

The altitude of the DEM was exaggerated 10 times before the classification, to enable the BTM to detect the shapes of the landscape. The fine- and broad scales were determined based on the BPI results for different radius sizes. The best results were obtained from a broad scale BPI of 100 m radius and a fine scale BPI of 10 m radius. The fine- and broad scale BPIs were used, together with DEM derived slopes to classify the investigated area into the geomorphometric classes: Small-scale crests, large-scale crests, depressions, slopes and flats (Fig. 4). The classification classes were decided based on previous studies using the BTM classification tool with success (Diesing et al., 2009; Lundblad et al., 2006). The thresholds for the fine- and broad scale BPIs were in previous

studies often defined as 1 standard deviation (Lundblad et al., 2006; Verfaillie et al., 2007), however, thresholds of 0.5 standard deviations have also previously been applied (Kaskela et al., 2012). We used a low threshold of 0.5 standard deviations due to the generally very gentle variations in the landscape geometry of the tidal inlet system. We defined the threshold between slopes and flats as 2°. This definition was a compromise between detecting as many slopes as possible but avoiding too many "false slopes" being detected along the swath edges, which seemed to be a consequence of lower precision at the outer beams of the swath, as well as differences between overlapping swaths.

Morphological classification analysis

A morphological classification was developed for the purpose of delineating classes of actual morphological features in the study area. This classification was built partly on different neighbourhood analyses and slopes derived from the DEM, and partly on the local tidal range. Large scale crests from the geomorphometric classification were also incorporated in the analysis.Figure 5 describes the steps performed in ArcGIS, which led to the classification of 6 morphological classes: Swash bars, linear bars, beach dunes, intertidal flats, intertidal creeks and subtidal channels. All the criteria for defining a particular morphological class had to be fulfilled for a cell to be classified into that class.

33 years of continuous measurements of the water level at Havneby on Rømø, 25 km south of the study area, shows a mean low water level of -0.94 m (DVR90) and a mean high water of 0.94 m (DVR90) (Klagenberg et al., 2008). Although the tidal range in Knudedyb is probably slightly different, it is the best estimate for the study site. Therefore, these water levels were used to separate between the supratidal, intertidal and subtidal zones.

Subtidal channels were defined as everything below the mean low water, which is -0.94 m. A "smooth DEM" was created, in which each cell of the original DEM was assigned the average altitude value of its surrounding cells in a window size of 100x100 m. The result was subtracted from the original DEM, creating an Elevation Change Model (ECM), which made it possible to extract information about the deviation of the cells in the DEM compared to its surrounding cells. The principle is similar to the BPI, and again the purpose was to locate cells, with a higher/lower altitude than its surrounding cells. Positive values were higher cells and negative values were lower cells. Certain thresholds were found suitable for classifying beach dunes (> 0.8 m) and intertidal creeks (< -0.3 m). These two classes were furthermore classified into their respective tidal zones

(supratidal and intertidal) based on the altitude. Intertidal flats were classified by low slope values (< 1°) of a down-sampled 2 m DEM (each down-sampled cell was assigned the mean value of its 4x4 original cells). Moreover, to be classified as a flat, the ECM has to be within ±10 cm to avoid any incorrect intertidal flat classification of flat crests on top of bars or flat bottoms inside creeks or channels. The BTM classification class "large-scale crests" is used as an input, since it is found to capture bar features. However, the thresholds used in the BTM classification resulted in capturing features larger than bars in the large-scale crests class. To distinguish between bars and larger features, the standard deviation of each DEM cell in a moving window size of 250x250 m is calculated. A suitable threshold to distinguish between bars and larger features are 0.6 standard deviations. Finally, swash bars and linear bars are distinguished by an area/perimeter-ratio, based on the assumption that linear bars has a smaller ratio than swash bars, due to the different shapes. In this case, 4 were found to be a suitable ratio threshold.

4 Results

4.1 Refraction correction and dead zone extent

The vertical adjustment of the LiDAR points due to refraction correction (z_{diff}) is linearly correlated with the water depth (d) (Fig. ~~5). The~~6). An empirical formula was derived for this relationship and is given by the equation:

$$z_{\text{diff}} = 0.227 * d\,,\ \mathrm{R}^2 = 0.997 \qquad (~~8~~7)$$

A LiDAR point at 1 m water depth is vertically adjusted by approximately 0.23 m (Fig. ~~5~~6). The variations around the linear trend in Fig. ~~5~~6 are due to changing incidence angles of the laser beam that varies with the airplane attitude (roll, pitch and yaw).

~~The dead zone is clearly visible in the LiDAR point cloud as a gap with no water points at very shallow water depths (Fig. 6).~~

The vertical extent of the dead zone is approx. 28 cm, determined by plotting the vertical difference between the shallowest and the deepest LiDAR point within 0.5 m cells – i.e. between the shallow surface and the deep surface (Fig. 7). The difference is manifested by an abrupt change ~~in~~at the dead zone, and the highest rate of change is shown to be at a water depth of approx. 28 cm.

4.2 Sub-decimetre accuracy and precision

The vertical ~~accuracy~~ root mean square error of the LiDAR data is ±4.1 cm, and the accuracy is ±8.1 cm with a 95% confidence level (Table ~~2~~1 and Fig. 8A). ~~This means that there is 95% likelihood for a given LiDAR point measurement to be within ±8.1 cm of the actual elevation at that position.~~ The vertical precision of the LiDAR data with a 95 % confidence level is ±3.8 cm for the points on the frame, and ±7.6 cm for the points on the block (Table ~~2~~1).

The horizontal accuracy calculated as the horizontal mean absolute error ($E_{\mathrm{MA,xy}}$) is determined to ±10.4 cm, which is the average of the minimum distances between the four block corners and the edge of the block surface derived by the LiDAR data (Fig. 8B).

4.3 Point density and resolution

The average point density is 20 points per m^2, which equals an average point spacing of 20 cm (Table ~~3~~2). The point density of the individual swaths varies between 7-13 points per m^2, and the point density of the combined swaths in the study area, varies between 0-216 points per m^2, although above 50 points per m^2 are rare.

~~The point density of the combined swaths varies significantly throughout the area, spanning between 0-216 points per m^2, although above 50 points per m^2 are rare (Fig. 8A). The highest point density is found in vegetated areas on Fanø, where a single laser pulse potentially returns multiple signals. The density on the tidal flat is generally a little lower. The local point density is, however and not surprisingly, highly related to the number of overlapping swaths, which is evident by comparing the point density (Fig. 9A) with the number of swath overlaps (Fig. 9B).~~

~~The large variation of the point density and its spatial relation to swath overlaps is also reflected by the frequency distribution of the point density (Fig. 10). Three peaks are visible in the distribution around 8, 17 and 26 points per m^2. They fit very well with the expected densities from 1, 2 and 3 overlaps, respectively, when keeping in mind the point density of the individual swaths.~~

4.4 DEM and landforms

The ~~elevations~~altitudes in the studied section of the Knudedyb tidal inlet system range from -4 m DVR90 in the deepest parts of the flood channel and main channel to 21 m DVR90 on top of the beach dunes on Fanø (Fig. ~~11~~9). Beach dunes and cottages of the village Sønderho are clearly visible in the northern part of the study site (Fig. ~~11A~~9A-B). The ~~tidal inlet system is~~intertidal areas

are generally flat, ~~with~~while the most varying morphology is found in the area of the flood channel (Fig. ~~11C~~9C-D), and in the area close to the main channel (Fig. ~~11E~~9E-F). The flood channel is approximately 200 m wide in the western part and it divides into two channels towards east. The bathymetry of the channel bed is clearly captured by the LiDAR ~~measurements~~data in the eastern part, and also in the western part down to -4 m DVR90, which approximately ~~equal~~equals a water depth of 3 m at the time of survey~~ time~~. An intertidal creek joins the flood channel from the north (Fig. ~~11D~~9D). From the flood channel towards south, the tidal flat is vaguely upward sloping, until reaching two distinct swash bars, which are rising 0.9 m above the surrounding tidal flat, reaching a maximum ~~elevation~~altitude of 1.5 m DVR90 (Fig. ~~11E~~9E-F). Further south, the linear bars along the margin of the main channel are clearly captured in the DEM (Fig. ~~11E~~9E).

4.5 Geomorphometric and morphological classifications

The geomorphometric and morphological classifications show that most of the study site is located in the intertidal zone, and is mostly flat. That is manifested by the dominating two classes; flats and intertidal flats (Fig. 10A-B). The geomorphometric classification identifies slopes as stripes with NNW-SSE directionality across the flats. These are following the direction of the survey lines, and thus, they are not real morphological features but more an indication of lower precision of the LiDAR data, especially at the outer beams of the swath. These swath artefacts are smoothed out in the morphological classification by down-sampling the DEM to 2 m resolution, and therefore, the intertidal flats appear uniform and seamless. The bar features close to the main channel are well defined in the geomorphometric classification where they are classified as large-scale crests and small-scale crests surrounded by slopes. In the morphological classification, these are identified based on neighbourhood analyses and separated by the area/perimeter-ratio into two classes, swash bars and linear bars (Fig. 10C). Large-scale crests are also found on Fanø in the northern part of the area, and most of these are classified as beach dunes in the morphological classification. The geomorphometric classification identifies more large-scale crests along the banks of the flood channel, however, these are not actual bar features but they are identified as crests due to the nearby flood channel and creeks resulting in a positive broad scale BPI. In the morphological classification it is possible to distinguish between these “false” crests and actual bar features, by looking at altitude deviations at an even larger scale than the broad scale BPI. The intertidal creek in the NWern part of the area is a mix of depressions, slopes and small-scale crests in the

geomorphometric classification, whereas it is relatively well defined and properly delineated in the morphological classification (Fig. 10D).

The geomorphometric classification identifies slopes along the banks of the main channel, flood channel and the intertidal creek, as well as in front of the beach dunes and along the edges of the swash bars and linear bars. The slopes seem particularly reliable at delineating the features in the intertidal zone; swash bars, linear bars and creeks. Depressions are primarily identified in the deepest detected parts of the main channel and in the flood channel, in the intertidal creek and in the beach dunes. Small-scale crests are found in the geomorphometric classification in locations which are high compared to its near surroundings. They are primarily seen as parts of the linear bars close to the main channel, in the beach dunes on Fanø and along the banks of the intertidal creeks.

A few small circular patches of approx. 5 m diameter with *Spartina Townsendii* (Common Cord Grass) located on the intertidal flat are classified as small-scale crests in the geomorphometric classification (Fig. 11). It clearly shows the capability of capturing relatively small features in the DEM and in the derived classification.

5 Discussion

~~5.1~~ Performance of the water surface detection

5.1 ~~The~~ method ~~for~~

The water surface in topobathymetric LiDAR surveys is most often detected from NIR LiDAR data, which is simultaneously collected along with the green LiDAR data (Collin et al., 2012; Guenther et al., 2000; Parker and Sinclair, 2012; Wang and Philpot, 2007). However, detecting the water surface based on the green LiDAR data provides a potential to perform topobathymetric surveys with just one sensor, thus optimizing the survey costs as well as data handling and storage.

The two critical issues ~~roser~~isen by Guenther et al. (2000), as mentioned in the introduction, concerning the water surface detection ~~assumes~~with green LiDAR were thoroughly investigated in this study. The first issue, regarding the gap of detected water surface signals in the dead zone, is addressed by detecting the water surface based on areas which are known to be covered by water, and thereafter extending the water surface until it intersects the topography, so that also the dead zone is covered by the ~~modeled~~modelled water surface. The second issue, regarding uncertainty in

the water surface altitude determination, is addressed using the results presented byMandlburger et al. (2013) who found a statistical relationship between the cloud of water surface points in the green LiDAR data and the water surface altitude derived from NIR LiDAR data. Mandlburger et al. (2013), however, did not describe the actual method of modelling the water surface, which is done in this study. Mandlburger et al. (2015), on the other hand, did propose a method for modelling the water surface, however, it was in a fluvial environment and the water level was based on manual determinations of cross sectional water levels. The water surface detection method in this study is thus new in combining the properties: 1) It is only using green LiDAR data, 2) it is based on automatic water level determination 3) it is applied in a tidal environment (can be applied in any coastal environment) and 4) it is open to the public and described in detail.

The developed water surface detection method is new but it must be pointed out that the assumption of a flat ~~surface, which is~~ water surface leaves room for improvements for the future, especially if it is applied in a fluvial environment. Assuming a flat water surface is indeed a simplification of the real world~~. The~~, since the water surface in reality can be inclined, and it can ~~also~~ be topped by waves. ~~An example~~

5.2 Implications of ~~wave action directly visible in~~ the ~~LiDAR point cloud~~dead zone

The vertical extent of the dead zone is ~~seen in~~ in this study determined to approx. 28 cm (Fig. ~~12.~~

~~The waves lead to a larger degree of uncertainty~~ 7), which means that no return signal is detected from the water surface when ~~determining the water surface level, however, the modelled water surface level in the example is in between the wave crests and troughs. Perhaps more important is the effect of the waves on the water surface angles and thereby the laser beam angles of incidence. It results in different~~ the water depth is less than 28 cm. As Guenther et al. (2000) explains, the dead zone poses a real challenge to the modelling of a water surface, because all submerged points, also those in less than 28 cm water depth, have to be corrected for refraction ~~angles than assumed with the horizontal surface. In order to account for this,~~. With the water surface ~~should include changing elevations and thereby form a complete surface model, including waves.~~

~~The water surface~~ detection method proposed in this work this issue has ~~an advantage~~been dealt with by extending the water surface into the dead zone, which makes it possible to correct ~~even~~ the LiDAR points in 0-28 cm water depth for refraction. ~~This~~In this way, the implication of the dead zone along the channel edges is diminished, which is particularly beneficial in ~~a~~ flat ~~area~~areas such

as the Knudedyb tidal inlet system, where the dead zone may cover large areas depending on the tide (Fig. ~~13~~12).

~~However, there are many~~The implication of the dead zone along the channel edges is minimised, but the setting is different for the small ponds ~~within the study site with a water surface in a~~ on the intertidal flats. They may have different ~~elevation~~water levels than in the large channels, but no detected water surface points, since the water depth in the ponds are generally less than the vertical extent of the dead zone, i.e. approx. 28 cm. The presented method is not capable of detecting a water surface in these ponds~~. This~~, which means that the bottom points of the ponds are not corrected for refraction. According to the ~~computed~~calculated refraction (Fig. ~~5~~6), omitting refraction correction of a 28 cm deep pond will result in -6 cm ~~elevation~~altitude error (naturally less error in shallower water). ~~For future investigations it will be an improvement if all the water surfaces are modelled. This could be achieved by implementing NIR LiDAR measurements in the LiDAR survey, since it is reflected by any water surface. It may also be achieved with green LiDAR as the only data source by detecting the returned signals reflecting off the water surface in the dead zone. Potentially, this could be achieved by analysing the waveforms and choosing the first local peak in the returned signal as a valid detected point. Thereby, both the sea bed and the water surface would have a seamless transition between land and water.~~

~~5.2~~5.3 ~~Quality~~Evaluation of the topobathymetric LiDAR data quality

The vertical accuracy of conventional topographic LiDAR has previously been determined to ±10-15 cm ~~(Hladik and Alber, 2012;Jensen, 2009;Klemas, 2012;Mallet and Bretar, 2009)~~(Hladik and Alber, 2012; Jensen, 2009; Klemas, 2013; Mallet and Bretar, 2009). Only few previous studies have focused on the accuracy of shallow water topobathymetric LiDAR data ~~(Nayegandhi et al., 2009;Steinbacher et al., 2012). Nayegandhi et al. (2009)~~(Mandlburger et al., 2015; Nayegandhi et al., 2009; Steinbacher et al., 2012). Nayegandhi et al. (2009) determined the vertical E_{RMS} of LiDAR data in 0-2.5 m water depth to ±10-14 cm, which is above the ±4.1 cm E_{RMS} ~~found in this study. Steinbacher et al. (2012)~~found in this study (Table 1). Steinbacher et al. (2012) compared topobathymetric LiDAR data from a RIEGL VQ-820-G laser scanner with 70 ground-surveyed river cross sections, serving as reference, and found that the system's error range was ±5-10 cm, which is comparable to the ±8.1 cm accuracy found in this study. Mandlburger et al. (2015) compared ground-surveyed points from a river bed with the median of the four nearest 3D-neighbors in the LiDAR point cloud, and they found a standard deviation of 4.0 cm, which is almost

equal to the ±4.1 cm standard deviation found in this study (Table 1). In comparison with these previous findings of LiDAR accuracy, the assessment of the vertical accuracy in this study indicates a good quality of the LiDAR data.

Mapping the full coverage of tidal environments, such as the Wadden Sea, require a combination of topobathymetric LiDAR to capture topography and shallow bathymetry and MBES to capture the deeper bathymetry. The two technologies make it possible to produce seamless coverage of entire tidal basins; however, merging the two products raises the question whether the quality of the data from the two different sources is comparable. Comparing the LiDAR accuracy with previous findings of accuracy derived from ~~multibeam sonar~~MBES systems indicates similar or slightly better accuracy from the ~~multibeam sonar~~MBES systems ~~(Dix et al., 2012;Ernstsen et al., 2006)~~(Dix et al., 2012; Ernstsen et al., 2006)~~. Dix et al. (2012) determined the vertical accuracy of a multibeam sonar by testing the system on different objects and in different environments, and found the vertical E_{RMS} to be ±4 cm. Furthermore, they tested a LiDAR system on the same objects and found a similar vertical E_{RMS} of ±4 cm. The vertical E_{RMS} of ±4.1 cm found in this study is very close to both the multibeam accuracy and LiDAR accuracy determined by Dix et al. (2012). Another study by Ernstsen et al. (2006) determined the vertical precision of a multibeam sonar based on 7 measurements of a ship wreck from a single survey. They found the vertical precision to be ±2 cm, which is slightly better than the vertical precision of ±3.8 cm (frame) and ±7.6 cm (block) found in this study.~~

~~Determining vertical accuracy and precision are standard practice in studies involving spatial data (FGDC, 1998;Graham, 2012;Jensen, 2009). Accuracy and precision are in many cases provided as single values, such as ±8.1 cm for the vertical accuracy in this case, and thereafter they represent the accuracy/precision of the whole dataset. However, the values actually only apply to the specific locations, where the assessment is conducted. In reality, the accuracy and precision may vary spatially, which is also the case by the differing precision of ±3.8 cm at the steel frame and ±7.6 cm at the cement block in this study. Furthermore, spatial variations of the precision throughout the study area are revealed by looking at the vertical difference between overlapping LiDAR measurements (Fig. 14).~~

. Dix et al. (2012) determined the vertical accuracy of MBES data by testing the system on different objects and in different environments, and found the vertical E_{RMS} to be ±4 cm. Furthermore, they tested a LiDAR system on the same objects and found a similar vertical E_{RMS} of ±4 cm. The

vertical E_{RMS} of ±4.1 cm found in this study is very close to both the MBES accuracy and LiDAR accuracy determined by Dix et al. (2012). Another study by Ernstsen et al. (2006) determined the vertical precision of a high-resolution shallow-water MBES system based on 7 measurements of a ship wreck from a single survey carried out in similar settings as the present study, namely in the main tidal channel in the tidal inlet just north of the inlet investigated in this study. They found the vertical precision to be ±2 cm, which is slightly better than the vertical precision of ±3.8 cm (frame) and ±7.6 cm (block) found in this study. Overall, accuracy and precision are within the scale of sub decimetres for both topobathymetric LiDAR and MBES systems, which enables the mapping of tidal basins with full coverage and with comparable quality.

Due to technical and logistical reasons, the data validation and the actual survey were carried out on different days and in different locations. Based on this, it is a fair question to ask, whether the determined quality actually represents the quality of the data within the study site. In order to address this issue, the environmental conditions between the two surveying dates, as well as the environmental differences, which may impact the data quality, between the study site and the validation sites are compared.

The environmental conditions in the two surveying days were similar, with sunny conditions, average wind velocities of 7-8 m/s (DMI, 2014) and significant wave heights, measured west of Fanø at 15 m water, of approx. 0.5 m coming from NW (DCA, 2014). However, the waves in the main channel, next to the study site, have been observed in the 30 May LiDAR point cloud to be not more than 0.2-0.3 m, which can be explained by the location of the study site in lee of the western most intertidal flats and the ebb-tidal delta. The wave heights in the rest of the study area (flood channel and intertidal ponds) were in the scale of sub decimetres. In comparison, there were no waves at validation site 2 in Ribe Vesterå River during the 19 April LiDAR survey. As already mentioned, the proposed water surface detection method has a shortcoming of not modelling the waves, and this is a source of error in areas exposed to waves. The precision of the seabed points within the study area are therefore expected to be worse than the ±3.8 cm precision determined at validation site 2, because of the larger wave exposure.

The water clarity/turbidity impacts the accuracy of the LiDAR data negatively, due to scattering on particles in the water column, which causes the laser beam to spread (Kunz et al., 1992; Niemeyer and Soergel, 2013). Moreover, part of the light is reflected in the direction of the receiver, and such return signals can be difficult to distinguish from the seabed return (Kunz et al., 1992). The

turbidity was measured at validation site 2 and in the flood channel close to the study site during the 19 April survey by collecting water samples and subsequently analysing the samples for suspended sediment concentration (SSC) and organic matter content (OMC). The analyses showed that the average SSC was higher in the flood channel (17.2 mg/kg) than in the river (10.2 mg/kg). In contrast, the average OMC was lower in the flood channel (25.5 %) than in the river (40.0 %). These observations indicate that 1) the underwater precision is assessed in a location with higher turbidity than the environment within the study site; therefore, the turbidity cannot be a cause of lower precision in the study site, and 2) the penetration depth seems to be controlled by the OMC rather than by the SSC. This is new knowledge, since no previous studies (from what we know) have investigated the relative effect of organic matter as opposed to inorganic matter on the laser beam penetration depth. However, in order to determine the relationship with statistical confidence, a more comprehensive study is needed, involving measurements of penetration depth at different SSCs and OMCs, and without disturbance from other environmental parameters.

5.4 Spatial variations of topobathymetric LiDAR data quality

The quality of spatial datasets is often provided as single values, such as ±8.1 cm for the vertical accuracy in this case, and then the determined value represents the accuracy/precision of the whole dataset. However, in reality the value is only a measure of the local quality at the location where the assessment is conducted. The quality of the dataset varies spatially, and one way to illustrate that is to extract the maximum vertical difference between the LiDAR points of the processed point cloud within every 0.5×0.5 m cell throughout the study site (Fig. 13). In flat areas, without multiple return signals, this shows the spatially varying precision of the dataset. There are large differences on Fanø, which is expected due to vegetation causing multiple LiDAR returns from both the vegetation canopy and from the bare ground. In contrast, the differences on the very ~~vaguely~~gently sloping, non-vegetated tidal flat ~~do not have a~~are up to 10 cm, and there is no simple and natural ~~explanation.~~reason for that variation. A range of ~~uncertainty~~ factors ~~are causing~~contribute to the observed variations:

Laser beam incidence angle: The incidence angle, at which the laser beam hits the ground/seabed, is determined by a combination of the scan angle, the water surface angle and the terrain slope. The shape of the footprint is stretched with larger incidence angles, and this effect can cause pulse timing errors in the detected signal, which leads to a decreasing vertical accuracy (Baltsavias, 1999). The error associated with larger scan angles is generally causing the outer beams, toward the

swath edges, to attain a lower accuracy (Guenther, 2007). This is a reason for the observed variations along the swath edges (Fig. 13). Terrain slopes has the same effect of decreasing the vertical accuracy due to the footprint stretching. The measured altitude tend to be biased toward the shallowest point of the slope within the laser beam (Guenther, 2007). However, the influence of slope is not crucial in the Knudedyb tidal inlet system, since it is generally a very flat area.

Vertical bias between overlapping swaths: Areas covered by more than a single swath~~, and hence constituting a higher point density,~~ tend to show more vertical variation in the LiDAR point measurements. ~~This is evident by comparing number of swath overlaps (Fig. 9B) and the local point density (Fig. 9A) with the local vertical difference of the LiDAR points (Fig. 14).~~

This can be caused by variance/error in the GPS measurements and/or IMU errors (Huising and Gomes Pereira, 1998). The vertical bias between swaths ~~is varying and it~~ has been observed in the point cloud to be up to 5 cm~~.~~, but it is varying throughout the study site. In most environments, a bias of 5 cm would be unnoticeable, but because of the large and very flat parts of the Knudedyb tidal inlet system, even a small bias becomes readily evident. ~~The bias between overlapping swaths may explain the lower precision at the block compared to the frame, because the block was covered by 7 swaths as opposed to 4 swaths at the frame. It seems counterintuitive that more overlapping swaths, leading to higher point density, eventually result in *lower* precision of the measurements. In this case, the difference between precision and accuracy should be kept in mind, and that the same relationship between overlapping swaths and accuracy does not necessarily exist.~~

~~Sloping areas: LiDAR measurements on sloping areas are expected to have lower vertical accuracy than on flat ground, because the laser beam footprint may span across different elevations. The exact position of the detected point can vary within the footprint, and thus it may also vary in elevation. Furthermore, the slope affects the footprint by increasing its area size and changing the shape to more elliptical and less round. The influence of slope is not crucial in the Knudedyb tidal inlet system, since it is generally a very flat area, but it is still an uncertainty factor to keep in mind.~~

~~Uncertainty with increased water depth: The accuracy and precision are expected to be lower as the laser beam penetrates deeper into the water column. It is first of all due to widening of the laser beam footprint, which means that the elevation of a single LiDAR point is derived from the measurement on a larger area on the sea bed. Secondly, any uncertainty associated to a LiDAR measurement is magnified with increasing water depth, due to the refraction correction. These~~

~~factors, together with slopes, are causing the LiDAR measurements to be less precise in the main channel and in the flood channel.~~

Water depth: The accuracy and precision are expected to be lower as the laser beam penetrates deeper into the water column (Kunz et al., 1992). The laser beam footprint is diverging as it moves through the water column, resulting in a larger footprint on the seabed. The altitude of the detected point is thus derived from the measurement on a larger area on the seabed, which will decrease the vertical accuracy, as well as decrease the capability of detecting small objects. With this in mind, the lower precision at the frame compared to the block is opposite of what would be expected, since the frame is below water and the block is on land. In this case, other factors, such as overlapping swaths and/or scan angle deviations, have more influence on the precision than the water depth. Also, it should be remembered that the frame surface was close to the water surface, and the effect of the water depth on the precision would most likely be more evident if it was located in deeper water.

Additional factors, beside the ones mentioned above, may ~~increase the uncertainty of~~influence the quality of LiDAR datasets. ~~This could for~~ For instance ~~be~~, a dense vegetation ~~covering~~cover of the ~~ground or sea bed,~~seabed or breaking waves~~, which~~ that makes ~~it~~ the laser detection of the seabed almost impossible ~~for the laser to detect the sea bed~~. However, these factors do not have a great influence in the studied part of the Knudedyb tidal inlet system, and thus they are not further elaborated. ~~Nevertheless, these factors must be taken into consideration for LiDAR surveys in different areas with lots of vegetation and slopes.~~

~~5.3~~5.5 ~~Impact~~Evaluation of the ~~findings~~morphological classification

The morphological classification presented in this study is based on the studied section of the Knudedyb tidal inlet system. The overall concept of using tidal range, slope and variations of the altitude at different spatial scales proves to be a reliable method for delineating the morphological features in this tidal environment. The concept, however, can be applied in other environments. The specific thresholds in the classification determined in this study may deviate in other areas. Morphological features of different sizes require steps of other spatial scales in the neighbourhood analyses to produce a successful classification. In the future the classification method will be improved by implementing an objective method for determining the scales, which can make it applicable in areas with different morphological characteristics. Such an objective scale

determination method is presented by Ismail et al. (2015), who determined the scales based on the variance of the DEM at progressively larger window sizes. In this way, the sizes of the morphological features are determining the scales for the classification.

5.6 Using topobathymetric LiDAR data to map morphology in a highly dynamic tidal environment

The study demonstrates the capability of green topobathymetric LiDAR to resolve ~~small~~fine-scale features, while covering a broad-scale tidal inlet system. Collecting topobathymetric LiDAR data with a high point density of 20 points/m^2 on average enables detailed seamless mapping of large~~-scale tidal inlet system. While bridging between spatial scales,~~ tidal environments, and the LiDAR data has further proved to maintain a high accuracy~~, which means that shallow water zones can be mapped with a high level of detail.~~. The combined characteristics of mapping with high resolution and high accuracy in a traditionally challenging environment provide many potential applications ~~to the society~~, such as mapping for purposes of spatial planning and management, safety of navigation, ~~or~~ nature conservation~~.~~, or morphological classification, as demonstrated in this study. The developed LiDAR data processing method is tailored to a morphological analysis application. The best representation of the morphology is mapped by gridding the average value of the LiDAR points into a DEM with a 0.5 × 0.5 resolution. Other applications would require different gridding techniques. For instance hydrographers, who are generally interested in mapping for navigational safety, would use the shallowest point for gridding. However, the overall method for processing the point cloud can be used regardless of the application. Only the last and least challenging/time consuming step of gridding the point cloud into a DEM may vary depending on the application.

~~During a single LiDAR survey, the present state of the environment is captured with high resolution and high accuracy. However, the coastal zone is a highly dynamic environment influenced by complex hydrodynamic processes and feedback mechanisms. Therefore, a continuous monitoring of the coastal zone with high accuracy LiDAR systems will provide an insight to the temporal variation, whether caused by climate variation or inflected by human activities.~~

Applying topobathymetric LiDAR data for morphological analyses in tidal environments enables a holistic approach of seamlessly merging marine and terrestrial morphologies in a single dataset. In order to map the morphology of tidal environments in full coverage, however, a combination of topobathymetric LiDAR and MBES swath data is required. The comparable quality and resolution

of LiDAR and MBES data gives a potential to map large scale tidal environments, such as the Wadden Sea, in full coverage and with high resolution and high accuracy.

6 Conclusions

A new method was developed for processing raw topobathymetric LiDAR data into a digital elevation model with seamless coverage across the land-water transition zone. ~~The point cloud processing is based on simple concepts, which are easily repeatable, and the processing steps are described in detail. The novel method~~ Specifically a procedure was developed for water surface detection utilizing automatic water level determination from only green LiDAR data in a tidal environment. The method relies on basic principles, and in general the entire processing method is described with a high level of detail, which makes it easy to implement for future studies. ~~Specifically, the~~ The water surface ~~is extrapolated, so that it also covers the "dead zone", which has been determined to be approx. 0-28 cm in the very shallow water. The method does~~detection method presented in this work did not ~~model the spatially changing water levels, such as waves~~take into account the variation in wave heights and ~~inclined surfaces.~~surface slopes, which therefore constitutes a challenge to be addressed in future studies.

The vertical accuracy of the LiDAR data was determined by object detection of a cement block on land to ±8.1 cm with a 95% confidence level. The vertical precision was determined at the cement block to ±7.6 cm, and ±3.8 cm at a steel frame, placed just below the water surface. ~~The difference between the two sites is an indication of spatial variations throughout the study area, largely influenced by biases between overlapping swaths.~~ The horizontal mean error was determined at the block to ±10.4 cm. Overall, vertical and horizontal precision is within sub decimetre scale.

A seamless topobathymetric digital elevation model was created ~~for~~in a 4~~ × ~~×0.85 km section in the Knudedyb tidal inlet system. An average point density of 20 points per m^2 made it possible to create an elevation model of 0.5~~ × ~~×0.5 m resolution without significant interpolation. The model extends down to water depths of 3 m, which was the maximum penetration depth of the laser scanning system at the given environmental conditions. Measurements of suspended sediment concentration and organic matter content indicate that the penetration depth is limited by the amount of organic matter rather than the amount of suspended sediment.

The vertical "dead zone" of the LiDAR data has been determined to be approx. 0-28 cm in the very shallow water.

A morphological classification method was developed for classifying the area into 6 morphological classes: swash bars, linear bars, beach dunes, intertidal flats, intertidal creeks and subtidal channels. The morphological classification method is based on parameters of tidal range, terrain slope, a combination of various statistical neighbourhood analyses with varying window sizes and the area/perimeter-ratio of morphological features. The concept can be applied in any coastal environment with knowledge of the tidal range and the input of a digital elevation model; however, the thresholds may need adaptation, since they have been determined for the given study area. In the future the classification method should be improved by implementing an objective method for determining thresholds, which makes it immediately applicable across different environments.

Overall this study has demonstrated ~~a high potential for~~ that airborne topobathymetric LiDAR ~~to bridge scales, i.e. to resolve small scale landforms at landscape scales, and to bridge environments, i.e. to close the gap between marine and terrestrial environments in the coastal zone or in other shallow~~is capable of seamless mapping across land-water transition zones ~~like rivers and lakes~~even in environmentally challenging coastal environments with high water column turbidity and continuously varying water levels due to tides. Furthermore, we have demonstrated the potential of topobathymetric LiDAR in combination with morphometric analyses for classification of morphological features present in coastal land-water transition zones.

Acknowledgements

This work was funded by the Danish Council for Independent Research | Natural Sciences through the project "Process-based understanding and prediction of morphodynamics in a natural coastal system in response to climate change" (Steno Grant no. 10-081102) and by the Geocenter Denmark through the project "Closing the gap! – Coherent land-water environmental mapping (LAWA)" (Grant no. 4-2015).

References

Al-Hamdani, Z., Alanen, U., Andersen, J. H., Bekkby, T., Bendtsen, J., Bergström, U., Bučas, M., Carlén, I., Dahl, K., and Daunys, D.: Baltic Sea marine landscapes and habitats-mapping and modeling, BALANCE Technical Summary Report, part 2/4, 2008.

Alexander, C.: Classification of Full-waveform Airborne Laser Scanning Data and Extraction of Attributes of Vegetation for Topographic Mapping, PhD Thesis, University of Leicester, 2010.

Allouis, T., Bailly, J. S., Pastol, Y., and Le Roux, C.: Comparison of LiDAR waveform processing methods for very shallow water bathymetry using Raman, near-infrared and green signals, Earth Surface Processes and Landforms, 35, 640-650, 2010.

Baltsavias, E. P.: Airborne laser scanning: basic relations and formulas, ISPRS Journal of Photogrammetry and Remote Sensing, 54, 199-214, 1999.

Brzank, A., Heipke, C., Goepfert, J., and Soergel, U.: Aspects of generating precise digital terrain models in the Wadden Sea from lidar–water classification and structure line extraction, ISPRS Journal of Photogrammetry and Remote Sensing, 63, 510-528, 2008.

Cavalli, M., and Marchi, L.: Characterisation of the surface morphology of an alpine alluvial fan using airborne LiDAR, Natural Hazards and Earth System Science, 8, 323-333, 2008.

Chauve, A., Mallet, C., Bretar, F., Durrieu, S., Deseilligny, M. P., and Puech, W.: Processing Full-Waveform LiDAR data: Modelling raw signals, Internatinal archives of Photogrammetry, Remote Sensing and Spatial Information Sciences, 2007.

Collin, A., Archambault, P., and Long, B.: Mapping the shallow water seabed habitat with the SHOALS, Geoscience and Remote Sensing, IEEE Transactions on, 46, 2947-2955, 2008.

Collin, A., Long, B., and Archambault, P.: Merging land-marine realms: Spatial patterns of seamless coastal habitats using a multispectral LiDAR, Remote Sensing of Environment, 123, 390-399, 2012.

DCA: Wave data - Fanø Bugt, http://kysterne.kyst.dk/pages/10852/waves/showData.asp?targetDay=30-05-2014&ident=3071&subGroupGuid=16406, last access: 9 March 2016, 2014.

Diesing, M., Coggan, R., and Vanstaen, K.: Widespread rocky reef occurrence in the central English Channel and the implications for predictive habitat mapping, Estuarine, Coastal and Shelf Science, 83, 647-658, 2009.

Dix, M., Abd-Elrahman, A., Dewitt, B., and Nash, L.: Accuracy Evaluation of Terrestrial LIDAR and Multibeam Sonar Systems Mounted on a Survey Vessel, Journal of Surveying Engineering, 138, 203-213, 10.1061/(ASCE)SU.1943-5428.0000075, 2012.

DMI: Vejr- og klimadata, Danmark - Ugeoversigt 2014 - 22, 26 Maj 2014 - 1 Juni 2014, http://www.dmi.dk/uploads/tx_dmidatastore/webservice/t/g/i/s/r/20140601ugeoversigt.pdf, last access: 9 March 2016, 2014.

Doneus, M., Doneus, N., Briese, C., Pregesbauer, M., Mandlburger, G., and Verhoeven, G.: Airborne laser bathymetry–detecting and recording submerged archaeological sites from the air, J Archeol Sci, 40, 2136-2151, 2013.

Ernstsen, V. B., Noormets, R., Hebbeln, D., Bartholomä, A., and Flemming, B. W.: Precision of high-resolution multibeam echo sounding coupled with high-accuracy positioning in a shallow water coastal environment, Geo-mar lett, 26, 141-149, 2006.

Graham, L.: Accuracy. Precision and all That Jazz, LiDAR Magazine, 2, 2012.

Guenther, G. C.: Airborne laser hydrography: System design and performance factors, DTIC Document, 1985.

Guenther, G. C., Cunningham, A. G., LaRocque, P. E., and Reid, D. J.: Meeting the accuracy challenge in airborne lidar bathymetry, EARSel, Dresden, 2000.

Guenther, G. C.: Airborne lidar bathymetry, Digital elevation model technologies and applications: The DEM users manual, 2, 253-320, 2007.

Hladik, C., and Alber, M.: Accuracy assessment and correction of a LIDAR-derived salt marsh digital elevation model, Remote Sens Environ, 121, 224-235, 2012.

Hofle, B., Vetter, M., Pfeifer, N., Mandlburger, G., and Stotter, J.: Water surface mapping from airborne laser scanning using signal intensity and elevation data, Earth Surface Processes and Landforms, 34, 1635, 2009.

Huising, E. J., and Gomes Pereira, L. M.: Errors and accuracy estimates of laser data acquired by various laser scanning systems for topographic applications, ISPRS Journal of Photogrammetry and Remote Sensing, 53, 245-261, http://dx.doi.org/10.1016/S0924-2716(98)00013-6, 1998.

Höfle, B., and Rutzinger, M.: Topographic airborne LiDAR in geomorphology: A technological perspective, Zeitschrift für Geomorphologie, Supplementary Issues, 55, 1-29, 2011.

IHO: IHO Standards for Hydrographic Surveys (S-44), 5th edition, International Hydrographic Bureau Monaco, 2008.

Ismail, K., Huvenne, V. A., and Masson, D. G.: Objective automated classification technique for marine landscape mapping in submarine canyons, Marine Geology, 362, 17-32, 2015.

Jensen, J. R.: Remote sensing of the environment: An earth resource perspective 2/e, Pearson Education India, 2009.

Kaskela, A. M., Kotilainen, A. T., Al-Hamdani, Z., Leth, J. O., and Reker, J.: Seabed geomorphic features in a glaciated shelf of the Baltic Sea, Estuarine, Coastal and Shelf Science, 100, 150-161, http://dx.doi.org/10.1016/j.ecss.2012.01.008, 2012.

Klagenberg, P. A., Knudsen, S. B., Sørensen, C., and Sørensen, P.: Morfologisk udvikling i Vadehavet: Knudedybs tidevandsområde, Kystdirektoratet, 2008.

Klemas, V.: Airborne remote sensing of coastal features and processes: An overview, J Coastal Res, 29, 239-255, ~~2012~~2013.

Kunz, G., Lamberts, C., van Mierlo, G., de Vries, F., Visser, H., Smorenburg, C., Spitzer, D., and Hofstraat, H.: Laser bathymetry in the Netherlands, EAR-SeL Advances in Remote Sensing, 36-41, 1992.

Lecours, V., Dolan, M. F. J., Micallef, A., and Lucieer, V. L.: A review of marine geomorphometry, the quantitative study of the seafloor, Hydrol. Earth Syst. Sci., 20, 3207-3244, 10.5194/hess-20-3207-2016, 2016.

Lefebvre, A., Ernstsen, V. B., and Winter, C.: Estimation of roughness lengths and flow separation over compound bedforms in a natural-tidal inlet, Cont Shelf Res, 61-62, 98-111, 10.1016/j.csr.2013.04.030, 2013.

Leica: Leica LiDAR Survey Studio flyer, available at: http://leica-geosystems.com/products/airborne-systems/software/leica-lidar-survey-studio, last access: 24 March 2016, Heerbrugg, Switzerland, 2015.

Lundblad, E. R., Wright, D. J., Miller, J., Larkin, E. M., Rinehart, R., Naar, D. F., Donahue, B. T., Anderson, S. M., and Battista, T.: A benthic terrain classification scheme for American Samoa, Marine Geodesy, 29, 89-111, 2006.

Mallet, C., and Bretar, F.: Full-waveform topographic lidar: State-of-the-art, ISPRS J Photogramm, 64, 1-16, 2009.

Mandlburger, G., Pfennigbauer, M., Steinbacher, F., and Pfeifer, N.: Airborne Hydrographic LiDAR Mapping-Potential of a new technique for capturing shallow water bodies, Proceedings of ModSim'11, 2011.

Mandlburger, G., Pfennigbauer, M., and Pfeifer, N.: Analyzing near water surface penetration in laser bathymetry-A case study at the River Pielach, ISPRS Annals of Photogrammetry, Remote Sensing and Spatial Information Sciences, 1, 175-180, 2013.

Mandlburger, G., Hauer, C., Wieser, M., and Pfeifer, N.: Topo-bathymetric LiDAR for monitoring river morphodynamics and instream habitats—A case study at the Pielach River, Remote Sensing, 7, 6160-6195, 2015.

Millard, R. C., and Seaver, G.: An index of refraction algorithm for seawater over temperature, pressure, salinity, density, and wavelength, Deep Sea Research Part A. Oceanographic Research Papers, 37, 1909-1926, http://dx.doi.org/10.1016/0198-0149(90)90086-B, 1990.

Mousavi, M., Irish, J., Frey, A., Olivera, F., and Edge, B.: Global warming and hurricanes: the potential impact of hurricane intensification and sea level rise on coastal flooding, Climatic Change, 104, 575-597, 10.1007/s10584-009-9790-0, 2011.

Nayegandhi, A., Brock, J., and Wright, C.: Small-footprint, waveform-resolving lidar estimation of submerged and sub-canopy topography in coastal environments, Int J Remote Sens, 30, 861-878, 2009.

Niemeyer, J., and Soergel, U.: Opportunities of Airborne Laser Bathymetry for the Monitoring of the Sea Bed on the Baltic Sea Coast, ISPRS J Photogramm, Remote Sensing and Spatial Information Sciences, 1, 179-184, 2013.

Optech: Optech HydroFusion Information Sheet, available at: http://www.teledyneoptech.com/wp-content/uploads/specification_hydrofusion.pdf, last access: 24 March 2016, Canada, 2013.

Parker, H., and Sinclair, M.: The successful application of Airborne LiDAR Bathymetry surveys using latest technology, OCEANS, 2012 - Yeosu, 2012, 1-4,

Pe'eri, S., and Long, B.: LIDAR technology applied in coastal studies and management, J Coastal Res, 1-5, 2011.

Pedersen, J. B. T., and Bartholdy, J.: Budgets for fine-grained sediment in the Danish Wadden Sea, Mar Geol, 235, 101-117, 2006.

RIEGL: LAS extrabytes implementation in RIEGL software - Whitepaper, ~~2012.~~RIEGL Laser Measurement Systems GmbH, available at: www.riegl.com/uploads/tx_pxpriegldownloads/Whitepaper_-_LAS_extrabytes_implementation_in_Riegl_software_01.pdf, last access: 24 March 2016, 2012.

RIEGL: Datasheet RIEGL VQ-820-G, RIEGL Laser Measurement Systems GmbH, available at: http://www.riegl.com/uploads/tx_pxpriegldownloads/DataSheet_VQ-820-G_2015-03-24.pdf, last access: 24 March 2016, 2014.

RIEGL: Data Sheet RiHYDRO, RIEGL Laser Measurement Systems GmbH, available at: http://www.riegl.com/uploads/tx_pxpriegldownloads/11_DataSheet_RiHYDRO_2015-08-24_01.pdf, last access: 24 March 2016, 2015.

Rinehart, R., Wright, D. J., Lundblad, E. R., Larkin, E. M., Murphy, J., and Cary-Kothera, L.: ArcGIS 8. x benthic terrain modeler: Analysis in American Samoa, Proceedings of the 24th Annual ESRI User Conference, San Diego, CA, Paper, 2004, 2004,

Sacchetti, F., Benetti, S., Georgiopoulou, A., Dunlop, P., and Quinn, R.: Geomorphology of the Irish Rockall Trough, North Atlantic Ocean, mapped from multibeam bathymetric and backscatter data, Journal of Maps, 7, 60-81, 2011.

Schmidt, A., Rottensteiner, F., and Soergel, U.: Classification of airborne laser scanning data in Wadden sea areas using conditional random fields, International Archives of the Photogrammetry, Remote Sensing and Spatial Information Sciences XXIX-B3, 161-166, 2012.

Steinbacher, F., Pfennigbauer, M., Aufleger, M., and Ullrich, A.: High resolution airborne shallow water mapping, International Archives of the Photogrammetry, Remote Sensing and Spatial Information Sciences, Proceedings of the XXII ISPRS Congress, 2012,

Su, L., and Gibeaut, J.: EXTRACTING SURFACE FEATURES OF THE NUECES RIVER DELTA USING LIDAR POINTS, ASPRS/MAPPS 2009 Fall Conference, San Antonio, Texas, November 16-19, 2009.

Verfaillie, E., Doornenbal, P., Mitchell, A. J., White, J., and Van Lancker, V.: The bathymetric position index (BPI) as a supprt tool for habitat mapping. Worked example for the MESH Final Guidance, 14 pp., 2007.

Wang, C.-K., and Philpot, W. D.: Using airborne bathymetric lidar to detect bottom type variation in shallow waters, Remote Sensing of Environment, 106, 123-135, 2007.

Wright, D., Lundblad, E., Larkin, E., Rinehart, R., Murphy, J., Cary-Kothera, L., and Draganov, K.: ArcGIS Benthic Terrain Modeler, Corvallis, Oregon, Oregon State University, Davey Jones Locker Seafloor Mapping/Marine GIS Laboratory and NOAA Coastal Services Center, Accessible online at: http://www.csc. noaa. gov/products/btm, 2005.

Table 1: Specifications of the RIEGL VQ-820-G topobathymetric airborne laser scanner (RIEGL, 2014).

Flight altitude	~ 400 m above ground
Swath width	~ 400 m
Scan pattern	Section of an ellipse – arc shape
Scan angle	20° ±1°
Laser wavelength	532 nm
Pulse width	1 ns
Laser beam footprint (diameter)	40 cm (at 400 m flight altitude)
Laser pulse repetition rate	Up to 520,000 Hz
Max. effective measurement rate	Up to 200,000 meas./sec.
Laser beam divergence	1 mrad
Typical water depth penetration	1 Secchi disc depth

~~Table 2:~~

Table 1: Vertical accuracy and precision of the LiDAR point measurements, in terms of minimum error (E_{min}), maximum error (E_{max}), standard deviation (σ), mean absolute error (E_{MA}), root mean square error (E_{RMS}) and the 95% confidence level ($Cl_{95\%}$).

Accuracy/ Precision	Object	Best-fit plane	# points n	E_{min} (cm)	E_{max} (cm)	σ (cm)	E_{MA} (cm)	E_{RMS} (cm)	$Cl_{95\%}$ (cm)
Accuracy	Cement block	GCPs	227	0.01	12.1	4.1	3.5	±4.1	±8.1
Precision	Cement block	Point cloud	227	0.04	12.9	3.9	2.8	±3.9	±7.6
Precision	Steel frame	Point cloud	46	0.02	5.5	2.0	1.6	±1.9	±3.8

Table ~~3~~2: LiDAR point spacing and density for all the 11 individual swaths, which covered the study area, and for the combined swaths.

Swath number	1	2	3	4	5	6	7	8	9	10	11	All
Point spacing (m)	0.30	0.30	0.36	0.31	0.36	0.32	0.37	0.29	0.35	0.36	0.28	0.20
Point density (pt./m^2)	10.8	10.8	7.8	10.2	7.5	9.6	7.2	11.7	8.0	7.8	12.7	19.6

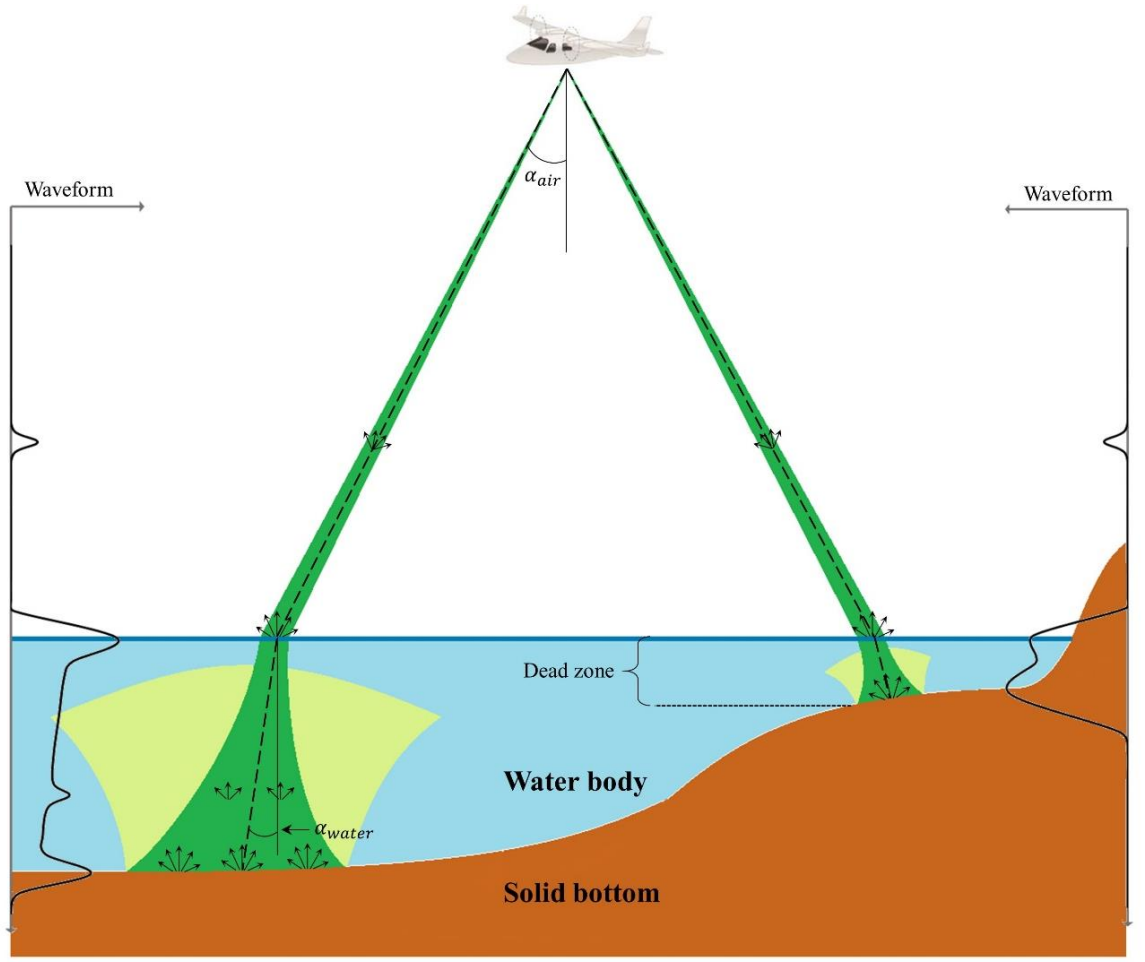

Figure 1: Conceptual sketch of the laser beam propagation and return signals. The beam refracts upon entering the water body, and it diverges as it propagates through the water column. Return signals are produced both in the air, at the water surface, in the water column and at the ~~sea bed~~seabed. The LiDAR instrument has limited capability in very shallow water (the "dead zone" in the figure) because the successive peaks from the water surface and the seabed are not individually separated in time and amplitude. Only the largest peak, which is from the ~~sea bed~~seabed, is detected.

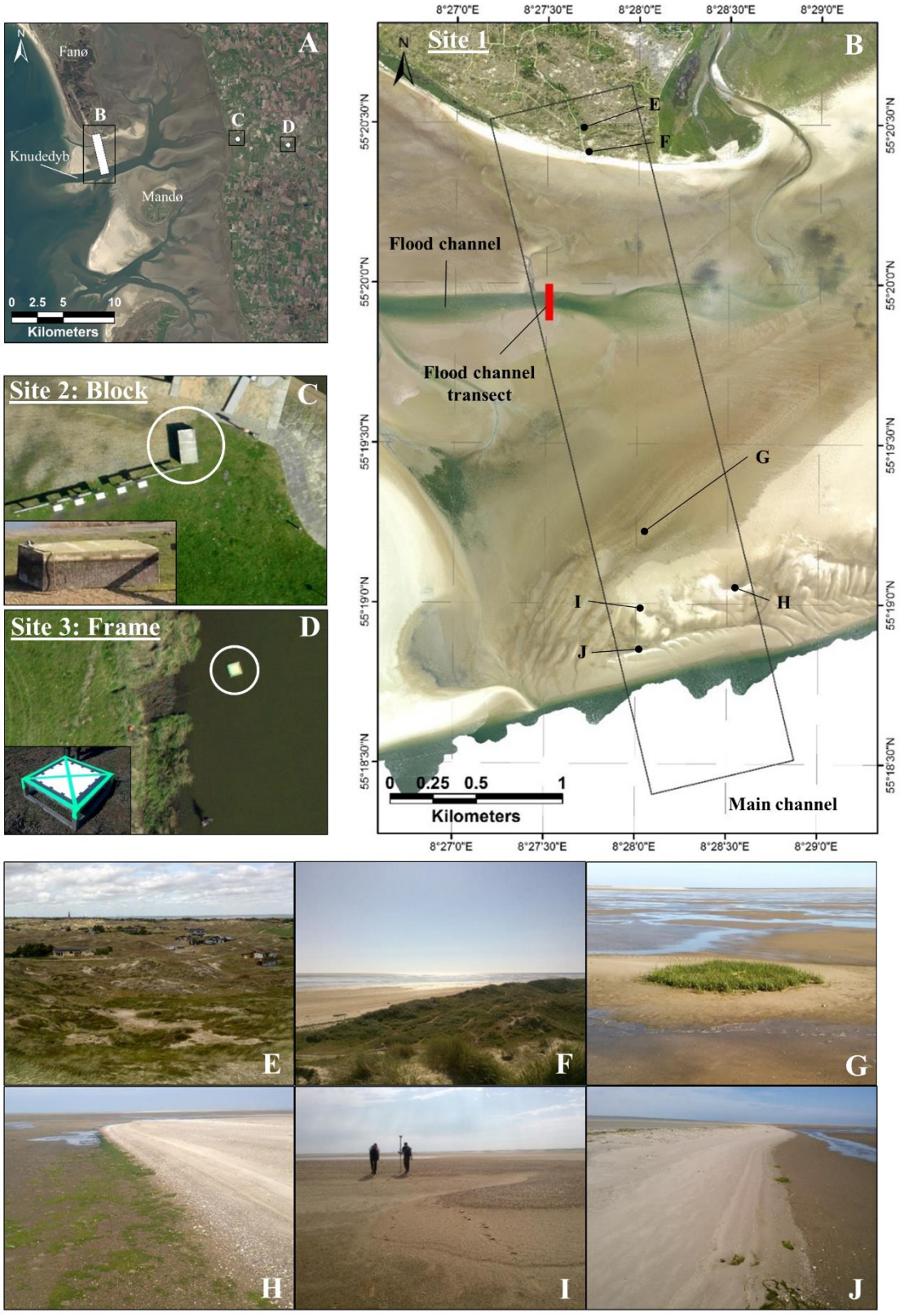
A
Fanø
B
C
D
Knudedyb
Mandø
0 2.5 5 10
Kilometers
Site 2: Block
C
Site 3: Frame
D
Site 1
B
E
F
Flood channel
Flood channel transect
G
I
H
J
0 0.25 0.5 1
Kilometers
Main channel
8°27'0"E
8°27'30"E
8°28'0"E
8°28'30"E
8°29'0"E
55°20'30"N
55°20'0"N
55°19'30"N
55°19'0"N
55°18'30"N
E
F
G
H
I
J

1

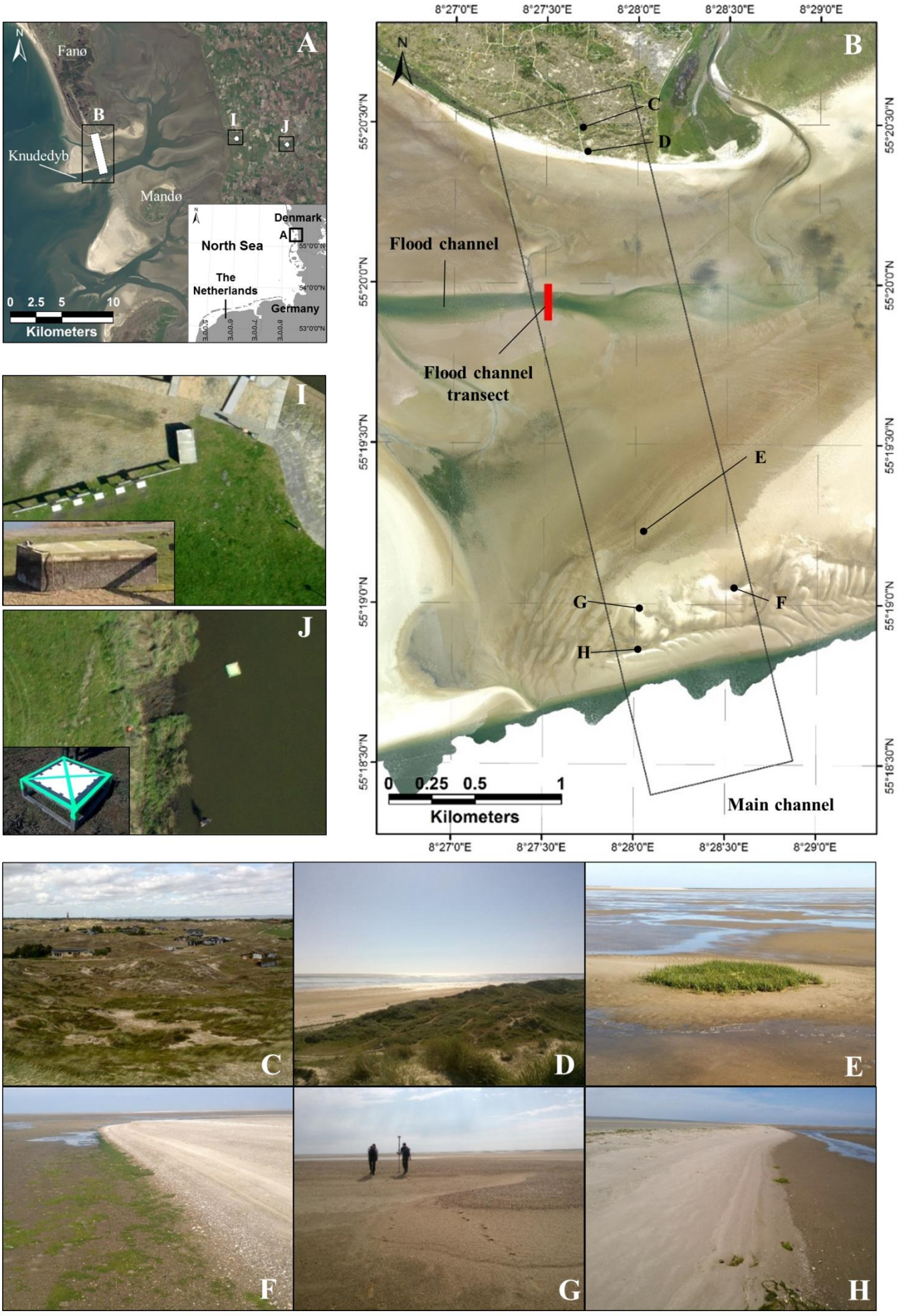
A
Fanø
B
Knudedyb
Mandø
I
J
Denmark
North Sea
The Netherlands
Germany
0 2.5 5 10
Kilometers
B
8°27'0"E
8°27'30"E
8°28'0"E
8°28'30"E
8°29'0"E
55°20'30"N
55°20'0"N
55°19'30"N
55°19'0"N
55°18'30"N
C
D
Flood channel
Flood channel transect
E
F
G
H
0 0.25 0.5 1
Kilometers
Main channel
I
J
C
D
E
F
G
H

Figure 2: A) Overview of the study area location in the Danish Wadden Sea and the specific locations of the study site (B) and the two validation sites (I and J) ~~three study sites~~ (22 April 2015 satellite image, Landsat 8). B) ~~Study~~The study site ~~1~~ in the Knudedyb tidal inlet system (30 May 2015 Orthophoto, AHM). ~~C) Study site 2~~C) Cottages in the dunes on Fanø. D) Beach dunes on Fanø. E) Patch of *Spartina Townsendii* (Common Cord Grass). F-G) Swash bars. H) Linear bar. I) Validation site 1 with a cement block on land, used for accuracy and precision assessment (19 April 2015 orthophoto, AHM). ~~D) Study~~J) Validation site ~~3~~2 with a steel frame in Ribe Vesterå River, used for precision assessment (19 April 2015 orthophoto, AHM). ~~E) Cottages in the dunes on Fanø. F) Beach dunes on Fanø. G) Patch of *Spartina Townsendii* (Common Cord Grass). H-I) Swash bars. J) Linear bar.~~

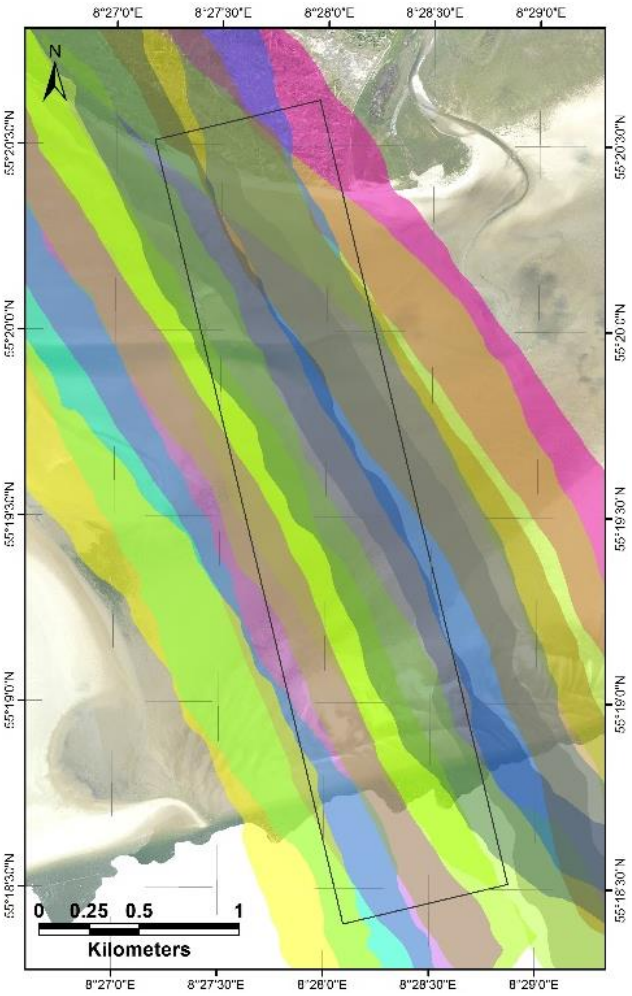

Figure 3: The 11 swaths covering study site 1, which were used for generating the DEM.

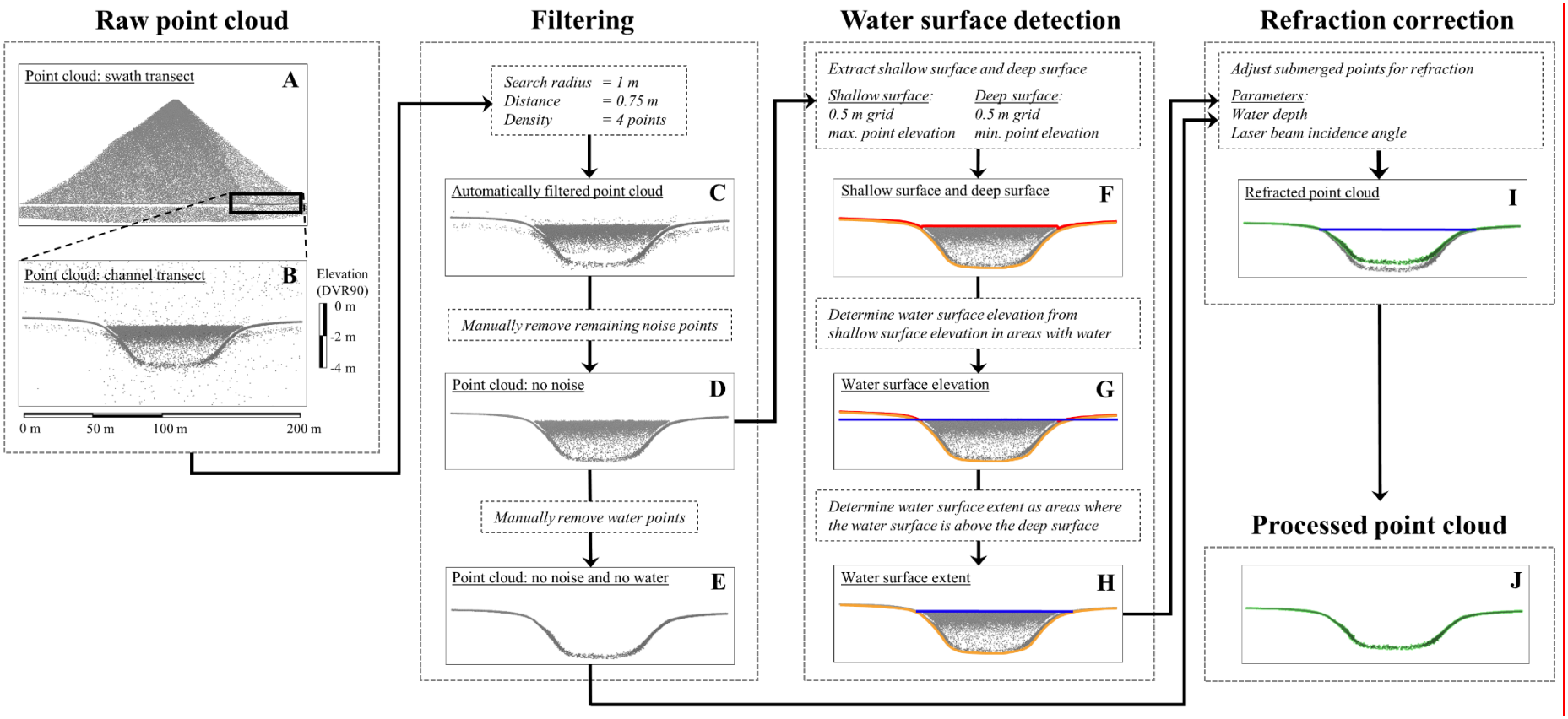

Figure 3: Workflow for processing the LiDAR point cloud. A) Point cloud from a single swath with points ranging from -100 m to 300 m elevation. B) Zoom-in on a cross section of the flood channel with altitudes exaggerated ×15 for visualization purpose. C-E) Method for filtering the point cloud. F-H) Method for detecting a water surface (blue) based on the extraction of a shallow surface (red) and a deep surface (orange). I) Correction for the effect of refraction on all the submerged points. J) Processed point cloud

1

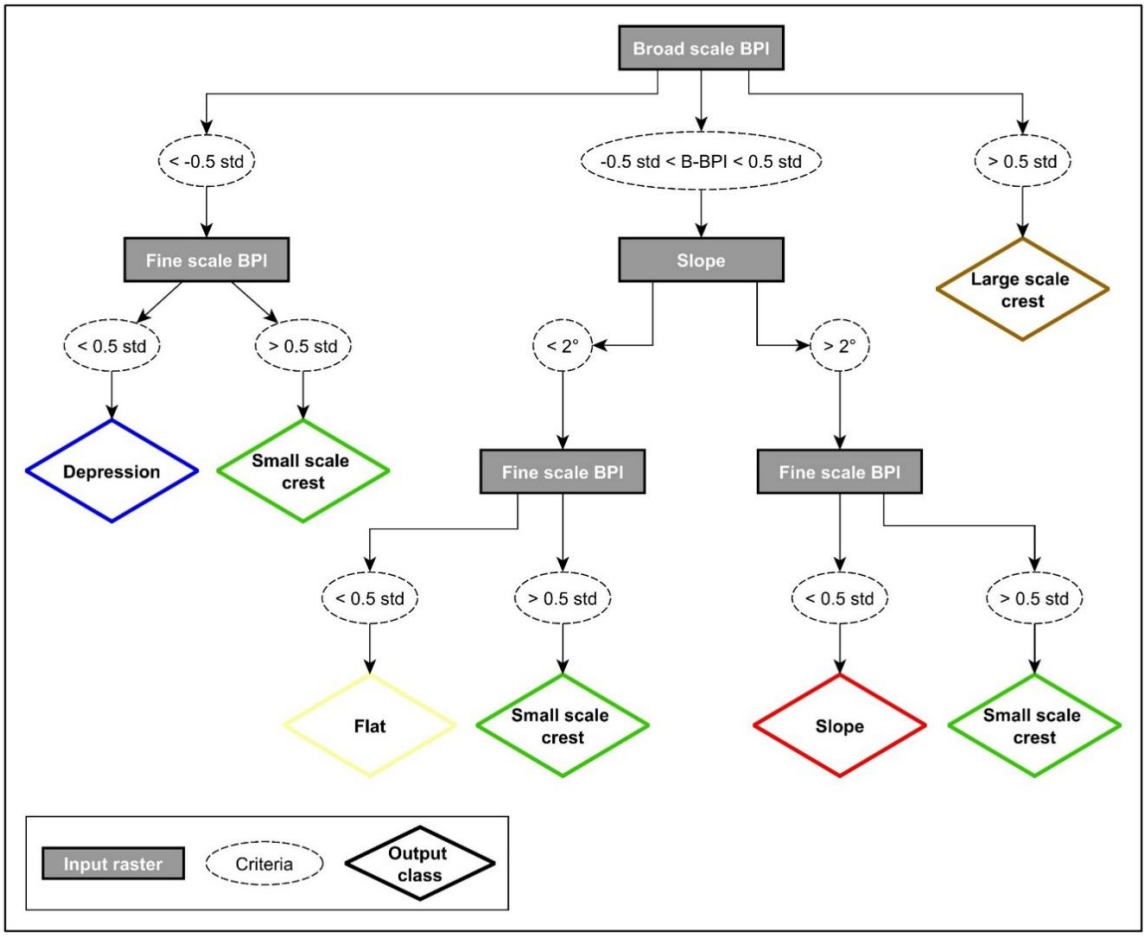

Figure 4: Classification decision tree, showing how the geomorphometric classification was conducted in the Benthic Terrain Model tool.

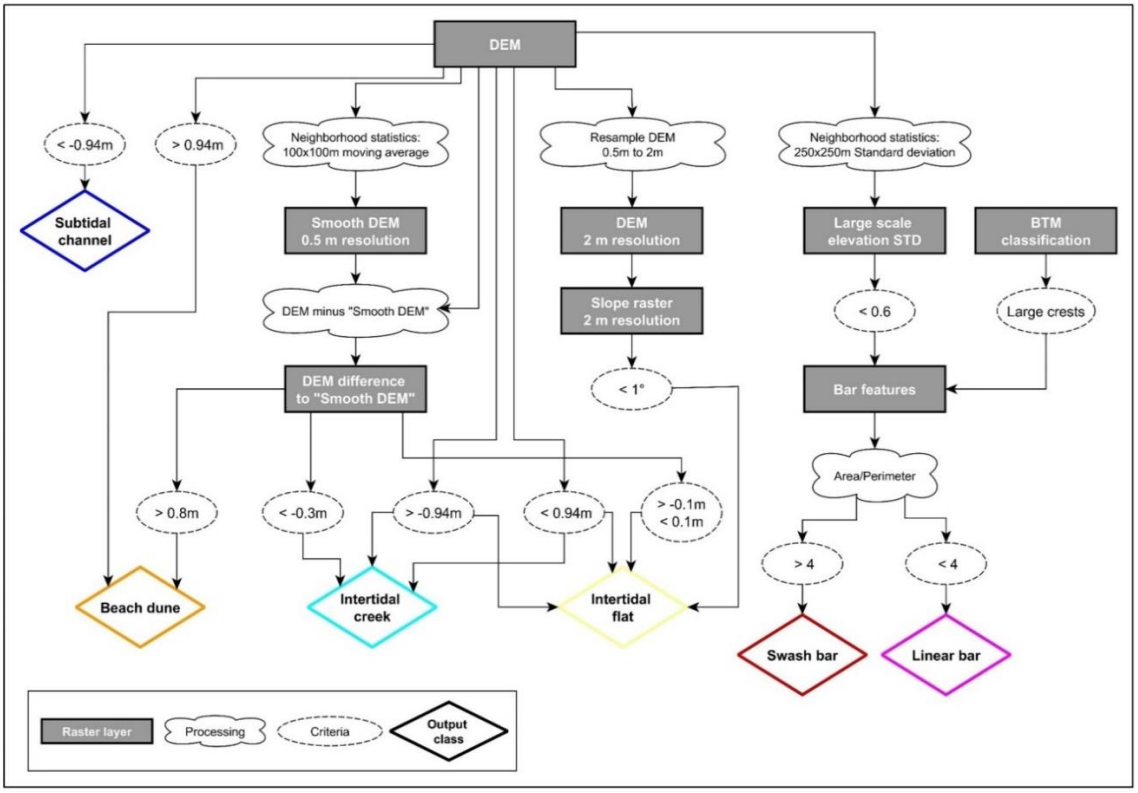

Figure 5: Classification decision tree of the morphological classification. All steps were performed in ArcGIS.

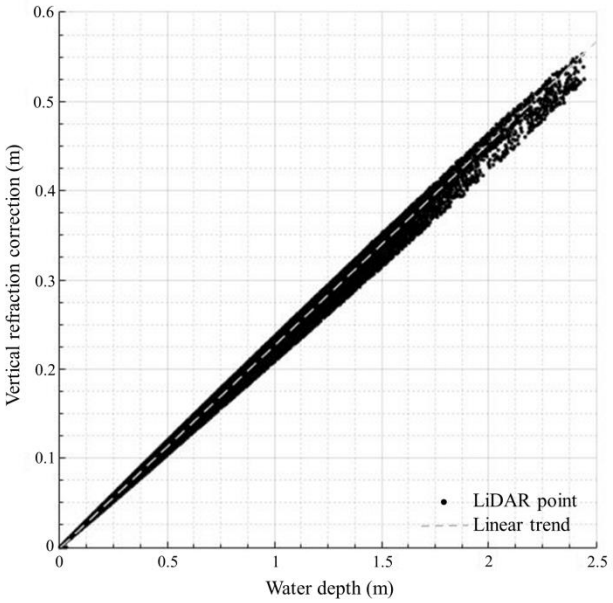

Figure ~~5.~~6: Vertical adjustment of the refracted LiDAR points from the flood channel transect (see location in Fig. 2C).

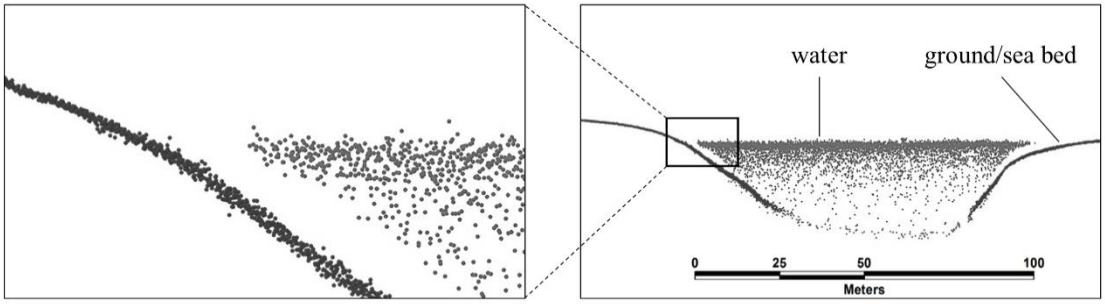

~~Figure 6: Example of a cross section of the flood channel, with a clearly visible gap in the water points in the very shallow water. The vertical dead zone is determined to be approx. 28 cm (see text).~~

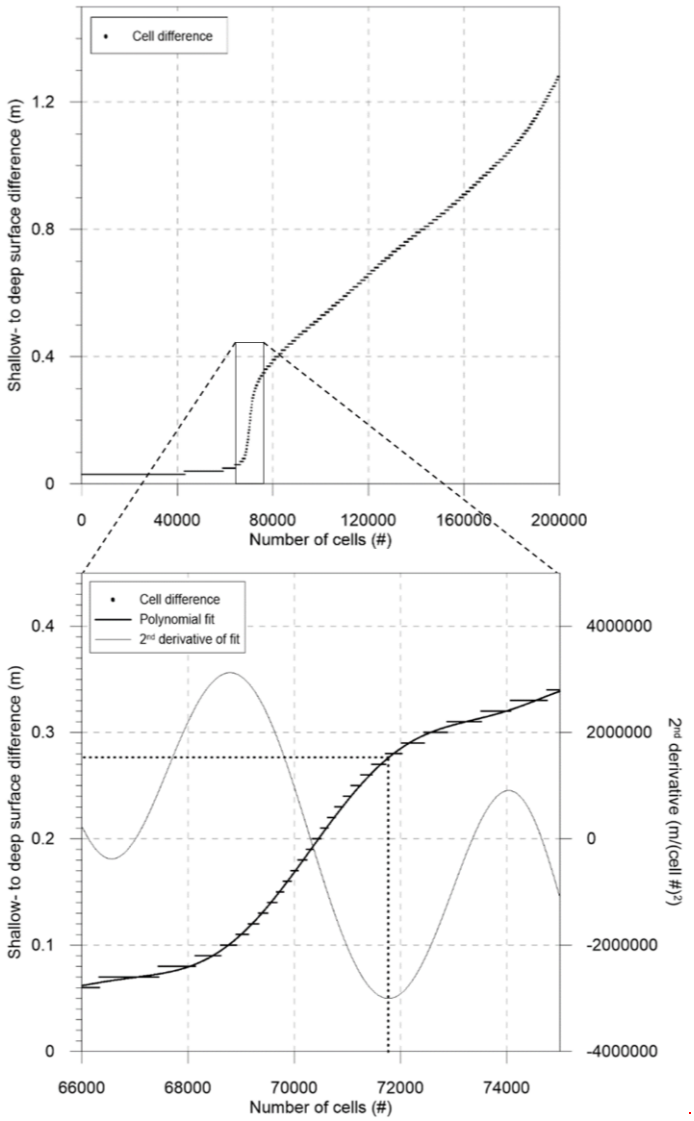

~~Figure 7:~~Figure 7: Vertical difference between the shallowest and the deepest LiDAR point within 0.5 m grid cells in the land-water transition zone. The abrupt change is caused by the dead zone. The vertical extent of the dead zone is determined to approx. 28 cm, derived by the maximum rate of change of a polynomial fit through the points.

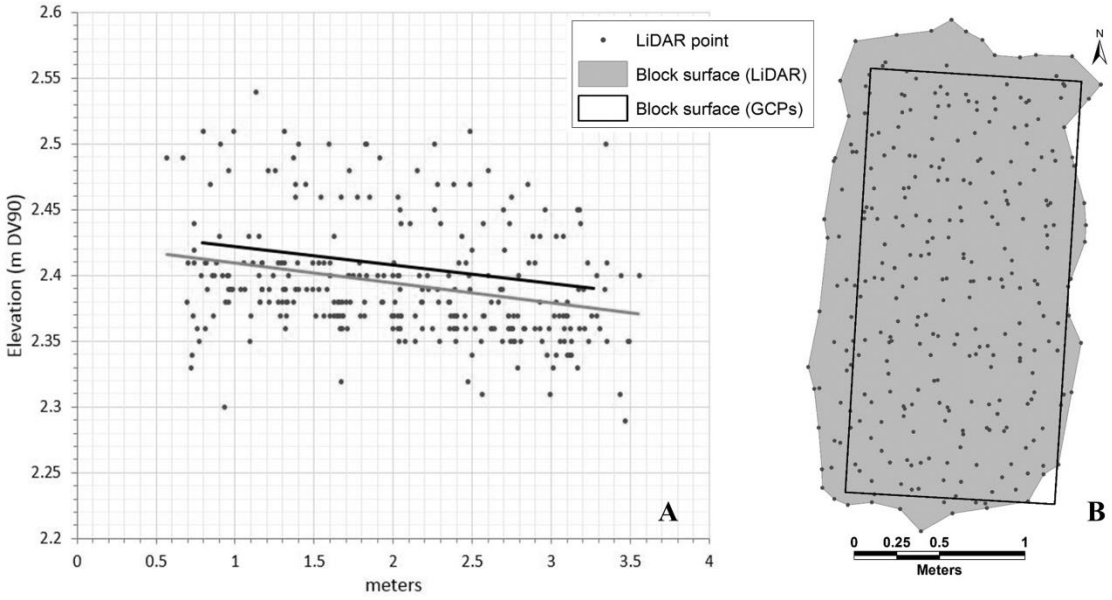

Figure ~~8.~~8: Vertical and horizontal distribution of the LiDAR points describing the block surface and the block surface derived from Ground Control Points (GCPs). A) LiDAR points (grey dots) compared to the GCP block surface (black line) for determining the vertical accuracy. The grey line shows the LiDAR block surface as a best-linear-fit through the points. B) Block surface derived from the four GCP corner points and the block surface derived by the perimeter of the LiDAR points.

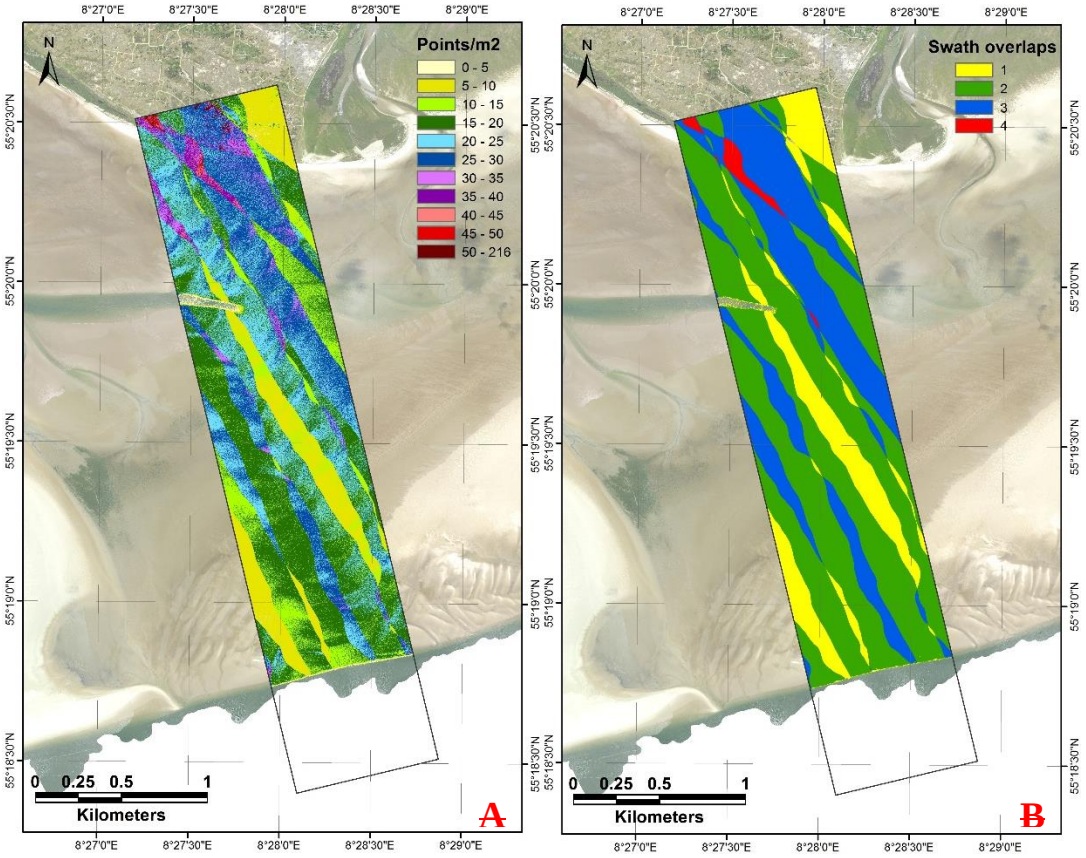

~~Figure 9: A) Point density (pts./m^2) throughout the study site. B) Number of swath overlaps in different sections of the study site.~~

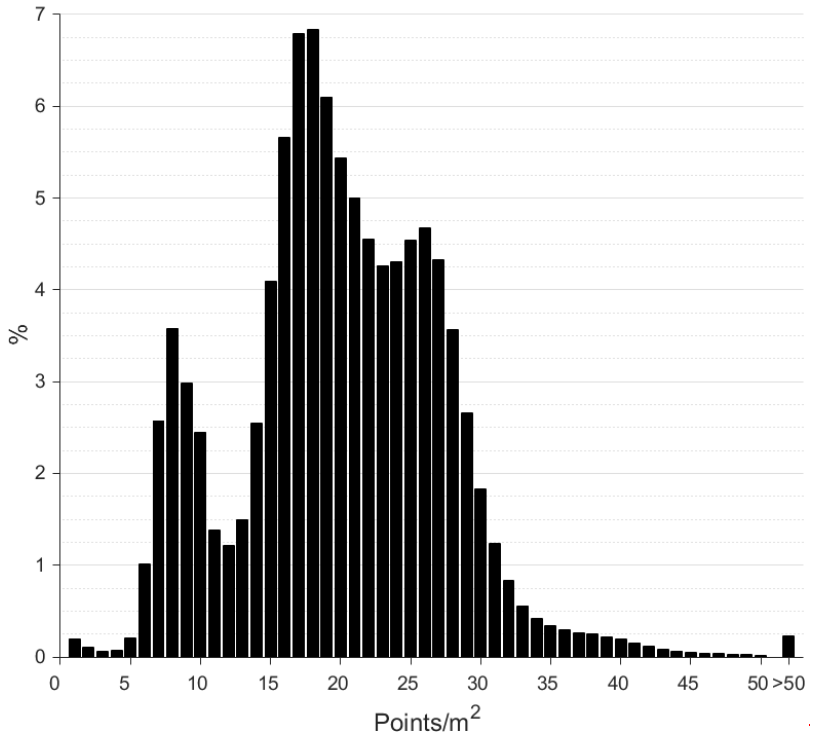

Figure 10: Frequency distribution of the varying LiDAR point density throughout the study area.

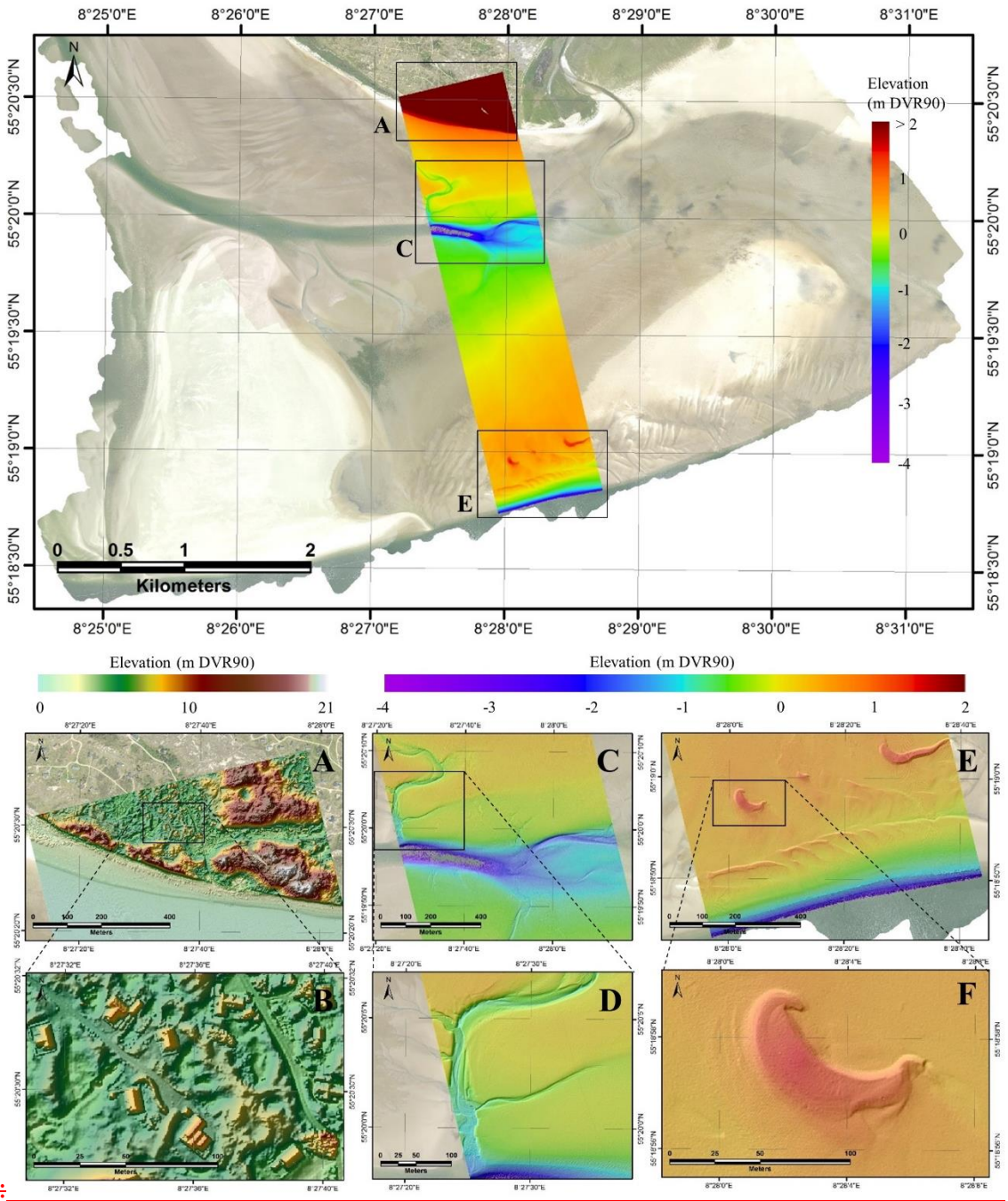

~~Figure 11:~~

Figure 9: Topobathymetric DEM across the northern part of the Knudedyb tidal inlet system with close-up views of different detail level on specific areas. A hill shade is draped upon the close-ups for improved ~~visual interpretation.~~visualization of morphological features. A) Northern section with beach dunes and cottages. B) Cottages. C) Mid-section with the flood channel. D) Closer view on an intertidal creek. E) Southern section with swash bars, linear bars and bathymetry of the main channel. F) Swash bar.

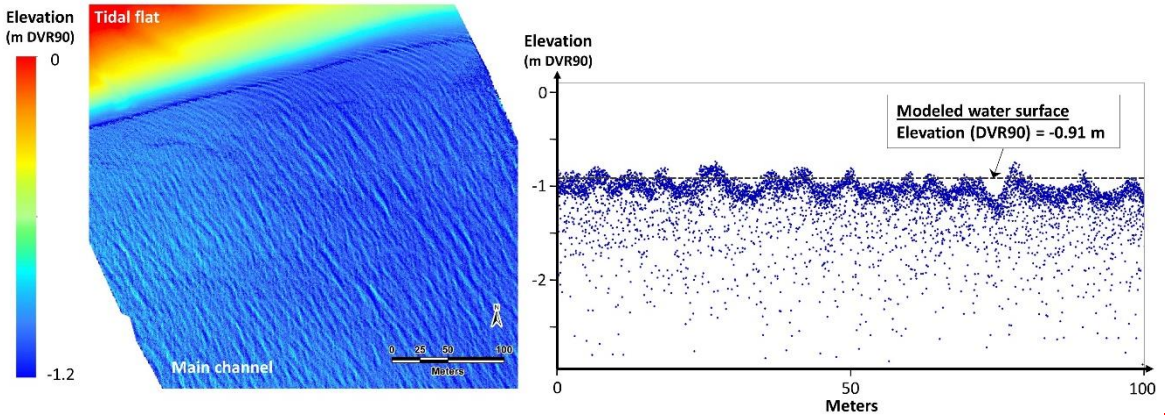
Elevation
(m DVR90)
0
-1.2
Tidal flat
Main channel
0 25 50 100
Meters
Elevation
(m DVR90)
0
-1
-2
Modeled water surface
Elevation (DVR90) = -0.91 m
0
50
100
Meters

1

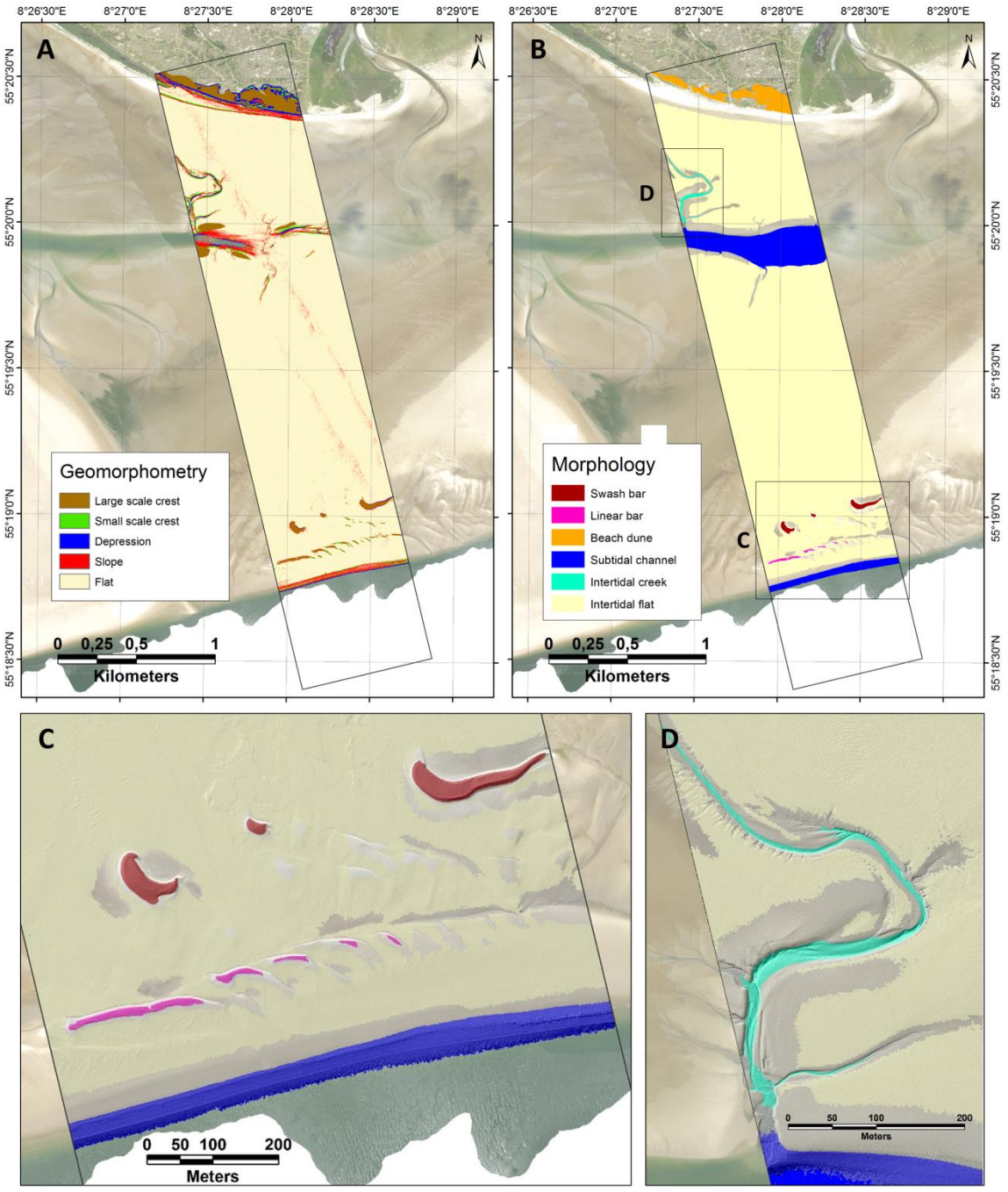

Figure ~~12: Examples~~10: Two classifications of ~~observed wave activity~~the investigated section in Knudedyb tidal inlet system, derived from a topobathymetric DEM. A) Geomorphometric classification. B) morphological classification. C) Zoom-in on the intertidal creek in the morphological classification. D) Zoom-in on the swash bars and linear bars close to the main channel in the ~~LiDAR data from a single swath. A)~~ morphological classification. A ~~vertical~~

~~view~~hillshade of the ~~shallow surface with 0.5 m resolution, showing waves near the tidal~~ DEM is draped over C and D.

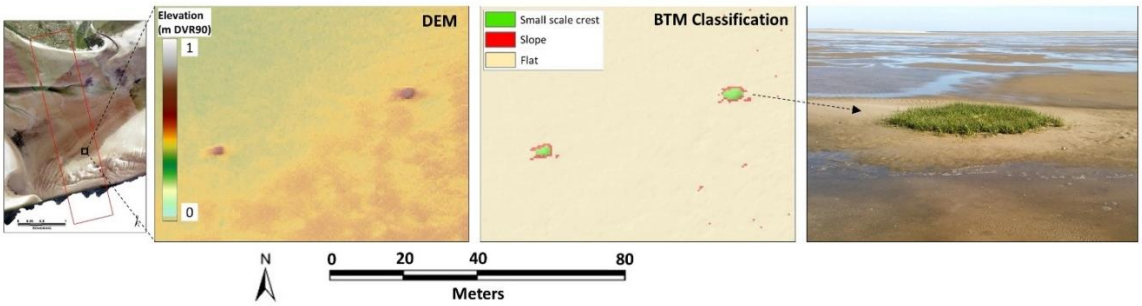

Figure 11: Vegetated mounds on the intertidal flat~~. B) A horizontal view along a transect through the point cloud, which~~ are clearly ~~captures the waves, together with the determined water surface.~~visible in the DEM and classified as small-scale crests in the geomorphometric BTM classification. To the right is an image of one of the patches.

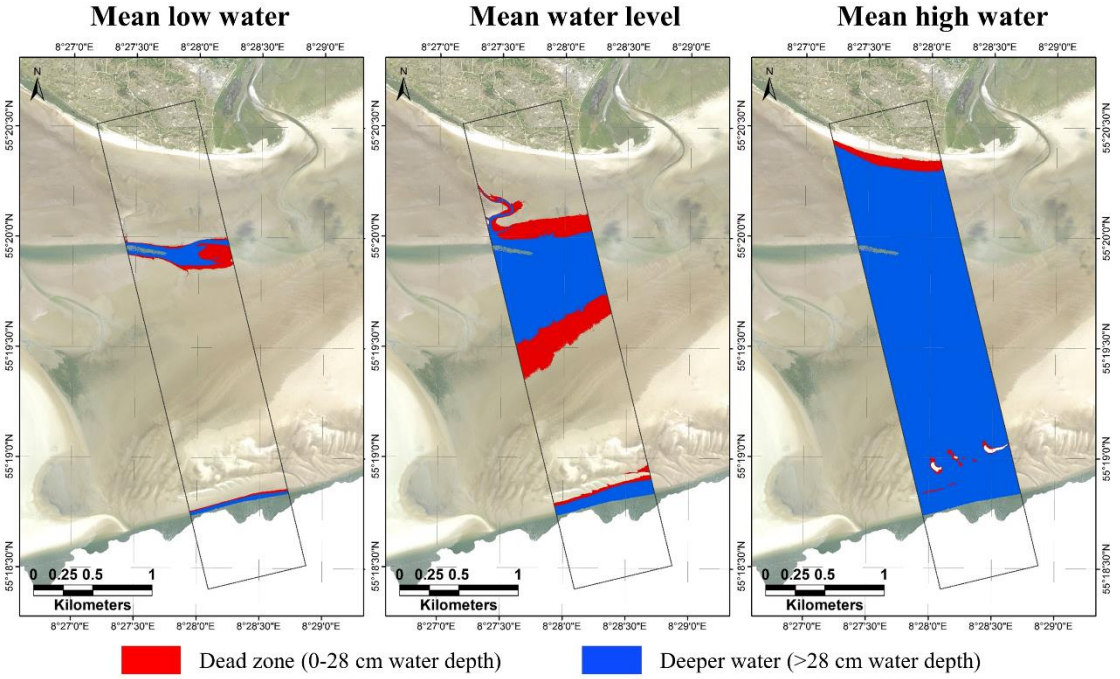

Figure ~~13.~~12: Horizontal extent of the dead zone in the studied area at mean low water, mean water level and mean high water.

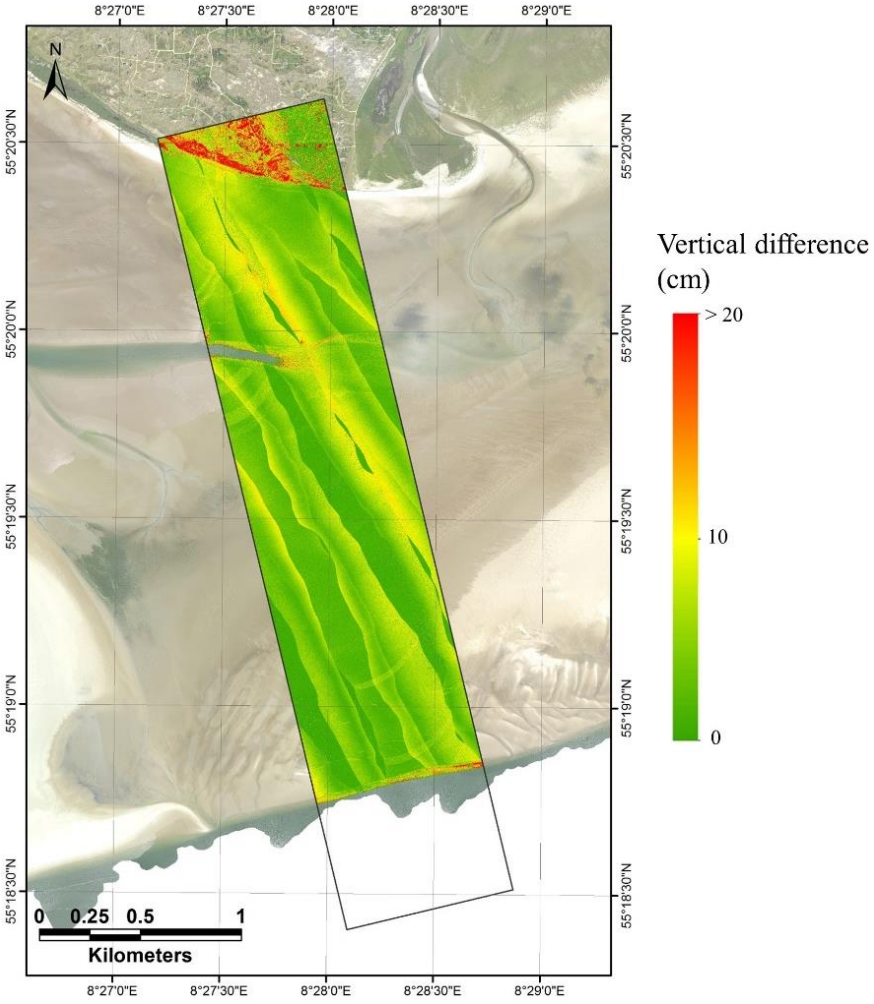

Figure ~~14:~~13: Vertical difference between the highest and the lowest LiDAR point within 0.5 ~~×~~ ×0.5 m grid cells.